Published in final edited form as:
Cell Calcium. 2009 September ; 46(3): 163–175. doi:10.1016/j.ceca.2009.07.001.

Metal-Controlled Interdomain Cooperativity in Parvalbumins

Sergei E. Permyakov[a,§,*], **Anush G. Bakunts**[a,§], **Maria E. Permyakova**[a], **Alexander I. Denesyuk**[a,b], **Vladimir N. Uversky**[a,c,*], and **Eugene A. Permyakov**[a]

[a]Institute for Biological Instrumentation of the Russian Academy of Sciences, Pushchino, Moscow region 142290 Russia [b]Department of Biochemistry and Pharmacy, Åbo Akademi University, Artillerigatan 6A, FI-20520 Turku, Finland [c]Institute for Intrinsically Disordered Protein Research, Center of Computational Biology and Bioinformatics, Department of Biochemistry and Molecular Biology, Indiana University School of Medicine, Indianapolis, Indiana 46202, USA.

Abstract

Conformational behavior of five homologous proteins, parvalbumins (PAs) from northern pike (α and β isoforms), Baltic cod, and rat (α and β isoforms), was studied by scanning calorimetry, circular dichroism, and bis-ANS fluorescence. The mechanism of the temperature-induced denaturation of these proteins depends dramatically on both the peculiarities of their amino acid sequences and on their interaction with metal ions. For example, the pike α-PA melting can be described by two successive two-state transitions with mid-temperatures of 90° and 120°C, suggesting the presence of two thermodynamic domains. The intermediate state populated at the end of the first transition was shown to bind Ca^{2+} ions, and was characterized by the largely preserved secondary structure and increased solvent exposure of hydrophobic groups. Mg^{2+} and Na^{+}-loaded forms of pike α-PA demonstrated a single two-state transition. Therefore, the mechanism of the PA thermal denaturation is controlled by metal binding. It ranged from the absence of detectable first-order transition (apo-form of pike PA), to the two-state transition (e.g., Mg^{2+} and Na^{+}-loaded forms of pike α-PA), to the more complex mechanisms (Ca^{2+}-loaded PAs) involving at least one partially folded intermediate. Analysis of isolated cavities in the protein structures revealed that the interface between the CD and EF subdomains of Ca^{2+}-loaded pike α-PA is much more loosely packed compared with PAs manifesting single heat-sorption peak. The impairment of interactions between CD and EF subdomains may cause a loss of structural cooperativity and appearance of two separate thermodynamic domains. One more peculiar feature of pike α-PA is that depending on its interactions with metal ions, it can be an intrinsically disordered protein (apo-form), an ordered protein of mesophilic (Na^{+}-bound state), thermophilic (Mg^{2+}-form), or even of the hyperthermophilic origin (Ca^{2+}-form).

*__CORRESPONDING AUTHORS:__ Sergei E. Permyakov, Institute for Biological Instrumentation of the Russian Academy of Sciences, Pushchino, Moscow region, 142290 Russia; Tel: 8(4967) 73 58 63; Fax: 8(4967) 33 05 22; permyakov.s@gmail.com; Vladimir N. Uversky, Center for Computational Biology and Bioinformatics, Department of Biochemistry and Molecular Biology, Indiana University School of Medicine, 410 W. 10th Street, HS 5009, Indianapolis, IN 46202, USA; Tel.: 317-278-9194; Fax: 317-274-4686; vuversky@iupui.edu.
§Equal contribution

Conflict of Interests
We confirm that there is no conflict of interest in this manuscript.

Keywords

thermodynamics; cooperativity; thermodynamic domain; structural domain; EF-hand; protein unfolding; protein denaturation; intermediate; metal binding; protein cavities; protein intrinsic disorder; hyperthermophile; allergen

1. Introduction

One of the fundamental properties of proteins, referred to as structural or global cooperativity, is their propensity to undergo concerted or independent conformational changes. Two limiting cases of structural cooperativity are known. One extreme is represented by small single-domain globular proteins. Such proteins typically possess rigid tertiary structure that favors cooperative structural rearrangements in response to changes in their environment, or as a result of the association with ligands or other binding partners. The melting of these proteins is described by a well-defined two-state transition, suggesting that a whole protein molecule serves as a single cooperative unit. Importantly, the reduction of structural cooperativity in small globular proteins may cause the appearance of partly unfolded intermediate states, ultimately leading to the formation and deposition of deleterious protein aggregates [1]. The appearance of stable intermediates in the course of protein folding can slow down the folding process [2].

The opposite extreme is represented by large proteins containing a series of structurally distinct domains, which fold and unfold independently from each other. This corresponds to a practically complete absence of structural cooperativity caused by the lack of the inter-domain interactions. The absence of structural cooperativity (interactions between domains) in large proteins may be advantageous for the fulfillment of several specific biological functions by the same protein molecule, as each domain can perform its function(s) (almost) independently of the nearby domains. Therefore, both extreme cases are important for protein functioning.

In addition to the aforementioned cases, the whole range of intermediate situations can be realized. Interestingly, some small globular proteins without distinct structural domains were shown to exhibit a complex multistage thermal denaturation behavior, suggesting the presence of multiple thermodynamic domains (for examples, see refs. [3,4]). Despite extensive studies, the factors governing structural cooperativity of small globular proteins are poorly understood as of yet. Such structural cooperativity is the characteristic feature of the naturally evolved proteins, as it is generally resistant for reproduction *in silico* and by the *de novo* design.

The known cases of the presence of multiple thermodynamic domains within small globular proteins can be regarded as manifestations of intrinsic properties of their polypeptide chains. Here we report a case when an additional thermodynamic domain is induced in a small globular protein, parvalbumin, as a result of metal ion-binding. Furthermore, we show that the mechanism of thermal denaturation can be controlled by the nature of the metal bound. A simple structural rationale for the appearance of an extra thermodynamic domain is derived based on the available structural data for closest relatives of this intriguing protein.

Parvalbumin is a small (Mr 10.5–12 kDa), acidic (pI 3.9–6.6), and cytosolic protein that belongs to the EF-hand superfamily of calcium binding proteins (for reviews see [5–8]). Parvalbumin is a vertebrate-specific protein, detected in fast-twitch muscle cells, specific neurons of the central and peripheral nervous system, certain cells of several endocrine glands, sensory cells of the mammalian auditory organ (Corti's cell), and some other cells. The highest concentration of parvalbumin (up to several millimoles per liter) was found in fast muscles (mainly in skeletal, but sometimes in cardiac) [9], and in the outer hair cells of Corti's cell [10]. Multiple studies [9,11–13] demonstrated that parvalbumin serves as a soluble relaxing factor accelerating the

Ca^{2+}-mediated relaxation phase in the fast muscles. The exact function of parvalbumin in non-muscle tissues is still mainly hypothetical. Nevertheless, its major role is assumed to be metal buffering, transport of Ca^{2+}, and regulation of various enzyme systems. Parvalbumin is widely used as a neuronal marker for a variety of functional brain systems and their circuitries (reviewed by Heizmann [14]). It is recognized as one of the major animal allergens [15,16]. Due to the presence of cross-reactive IgE epitopes, parvalbumin represents a cross-reactive fish allergen [17]. The extremely high stability of the calcium-loaded parvalbumin results in sensitization of patients despite high temperature cooking and exposure to the gastrointestinal tract environment [18,19].

The parvalbumin family includes two evolutionary distinct sublineages, α and β (the latest includes oncomodulin), distinguished by isoelectric point (pI>5 for α; pI<5 for β), C-terminal helix length (with few exceptions, one residue longer in α lineage), and several lineage-specific sequence identities [20,21]. Fish species have been shown to display up to eleven parvalbumin isotypes (African catfish [22]), distinct physiological roles of which are unknown as of yet. The age-dependent expression of PA isotypes was reported in various fish types [22,23]. This variability was attributed to the difference in the specific requirements for the physiological adaptations of the propulsive musculature related to fish size and performance (locomotion, feeding, etc) at various developmental stages of the growing fish.

The tertiary structure of parvalbumin is sublineage-independent and conserved over a wide phylogenetic range, demonstrating a high content of α-helices (six helical segments, labeled A to F), limited β-sheet structure, and no disulfides (reviewed in [8]). Parvalbumin consists of three homologous 30-residue-long subdomains, each containing central loop flanked by short amphipatic α-helices. The loops between the C and D helices and between E and F helices with flanking helices form two EF-hand type Ca^{2+}/Mg^{2+}-binding motifs (CD and EF subdomains). The AB subdomain is non-functional because of a two-residue deletion in the loop between the A and B helices. It covers the hydrophobic surface of the functional domains pair, thereby modulating their calcium affinities [24,25].

In the present work, the detailed studies of thermal denaturation of several representatives of the PA family revealed that Ca^{2+}-loaded parvalbumins were characterized by a complex denaturation mechanism, in some cases degenerating to two successive transitions of the “all-or-none” nature. The exchange of bound calcium ions in parvalbumin for magnesium or sodium ions changed the thermal denaturation mechanism, converting it into a single two-state process. Different lines of experimental evidence converged to the conclusion that the intermediate state, which appeared in the course of thermal denaturation of Ca^{2+}-loaded PA, is stabilized by Ca^{2+} ions. The analysis of isolated cavities in the protein structure and per-residue order/disorder predictions showed that the interface between the metal-binding domains of PA represented a boundary between the two thermodynamic domains.

2. Materials and Methods

2.1. Materials

Northern pike (*Esox lucius*) skeletal muscle PAs (α and β isoforms) were isolated as described earlier [26–28]. In our previous work, we have found two variants of pike α-PA, α_1 and α_2, differing by three residues (K27A, L31K, and an extra Leu between K11 and K12, in α_1-PA) [28]. All experiments in the present work were performed with α_1-isoform (which will be referred to as “α-PA”).

The rat (*Rattus norvegicus*) PAs were purified using the previously described procedure [29] with the following modifications. *Lac*-driven expression vectors pRV6 and pLD2 (derivatives of pBluescript II SK^+) were used for expression of recombinant rat PAs α and β, respectively.

The PA plasmids were kindly provided by Prof. Michael T. Henzl (University of Missouri). The purification scheme for rat α-PA was analogous to that described for the β isoform. *E. coli* DH10B cells, carrying the pLD2 expression vector, were grown in LB broth containing ampicillin (100 μg/ml) at 37°C until the growth (monitored by absorbance at 600 nm) reached the early stationary-phase. The cells were collected by centrifugation at 4°C, 5000×g for 15 min, and stored at −18°C. The cells were lysed in 50 mM Tris-HCl, 1 mM PMSF, 5 mM DTT, pH 7.4 by sonication (Branson Sonifier 450) on ice for 30 min. The lysate was kept at 4°C under stirring for 30 min, followed by centrifugation at 4°C, 5000×g for 30 min. 1 mM $CaCl_2$ was added to the supernatant. The solution was heated up to 80°C, maintained at 80°C for 3 min, immediately cooled using ice-water bath and centrifuged at 4°C, 15500×g for 30 min. The supernatant was dialyzed (MWCO 3.5 kDa) at 4°C against distilled water, followed by dialysis against 20 mM HEPES, pH 7.4. The dialyzed solution was loaded onto DEAE-cellulose column (2.6×10 cm) equilibrated with 20 mM HEPES, pH 7.4. Rat β-PA was eluted with a linear NaCl gradient (250 ml of 0 mM NaCl – 250 ml of 300 mM NaCl); elution rate was 1.2 ml/min. The fractions, containing rat β-PA, were collected, concentrated via freeze-drying, followed by dialysis (MWCO 3.5 kDa) at 4°C against 20 mM HEPES, pH 7.4. The remaining contaminants were removed by gel-filtration on Sephadex G-75 (5×27 cm) in 20 mM HEPES, pH 7.4; elution rate was 1.2 ml/min. The fractions containing rat β-PA were collected, concentrated via lyophilization, exhaustively dialyzed (MWCO 3.5 kDa) against distilled water at 4°C, freeze-dried, and stored at −18°C.

The purity of the protein samples was confirmed by native and SDS-PAGE, and checked spectrophotometrically, fluorimetrically and using circular dichroism spectroscopy. The parvalbumin concentration was determined spectrophotometrically using molar extinction coefficients of ε_{259nm}=1,810 $M^{-1}cm^{-1}$ and ε_{259nm}=2,699 $M^{-1}cm^{-1}$ for pike PAs α and β, respectively [30], ε_{280nm}=7,115 $M^{-1}cm^{-1}$ for cod PA (calculated according to [31]), ε_{258nm}=1,600 $M^{-1}cm^{-1}$ and ε_{274nm}=3,260 $M^{-1}cm^{-1}$ for rat PAs α and β, respectively [32].

HEPES, H_3BO_3 and glycine, ultra-grade, were from Sigma Chemical Co. (St. Louis, MO), Merck Biosciences, and Fluka, respectively. Tris and MES were purchased from Panreac Química S.A. and Sigma Chemical Co., respectively. Sephadex G-25 and G-75 were products of Pharmacia LKB and Whatman supplied DE52. Guanidinium chloride was biochemistry grade from Merck Biosciences; EDTA standard solution was from Fisher Scientific; $CaCl_2$ standard was from Fluka. Ultra-grade NaCl was from DiaM (Moscow, Russia). Molecular mass markers for SDS-PAGE were purchased from Helicon (Moscow, Russia). Silver staining of SDS-PAAG electrophoresis gels was carried out using Amersham Biosciences PlusOne™ protein silver staining kit. Other chemicals were reagent grade or higher. All buffers and other solutions were prepared using nano-pure water (Millipore Simplicity 185 system).

2.2. Apo-form preparation

The purification of parvalbumin samples from calcium ions was performed using the Sephadex G-25 gel-filtration method described by Blum *et al.* [33].

2.3. Scanning calorimetry

The scanning calorimetry measurements were carried out on a DASM-4M differential scanning microcalorimeter (IBI RAS, Pushchino, Russia) at a 1°C/min heating rate in 10–20 mM H_3BO_3 or glycine buffer, pH 8.1–9.0. A pressure of 3 bars was maintained in order to prevent degassing and boiling of the solutions during heating. The protein concentrations were 0.7–2.6 mg/ml. The heat-sorption curves were baseline corrected. The protein specific heat capacity (C_p) was calculated as described by Privalov and Potekhin [34]. The partial molar volume of PA and specific heat capacity of the fully unfolded protein were estimated according to Hackel *et al.* [35] and Makhatadze *et al.* [36], respectively. The temperature dependence of C_p was

analyzed according to either the *cooperative two-state model* [1] or the *model of two successive cooperative transitions* [2]:

$$n \cdot N \leftrightarrow n \cdot D \quad [1]$$

$$n \cdot N \leftrightarrow n \cdot I \leftrightarrow n \cdot D, \quad [2]$$

where N, I and D denote native, intermediate and denatured protein states, respectively; n is a number of molecules involved in the transition (cooperativity of thermal transition).

The experimental data were fit using Microcal OriginPro 8.0 (OriginLab Corporation, Northampton, MA) software. The heat capacity changes accompanying transitions were supposed to be independent of temperature. The cooperative two-state model [1] was described with the following expression (all values were normalized by protein molecular weight, MW), derived elsewhere:

$$C_p=(C_{p,N}+K \cdot C_{p,D})/(1+K)+\left[\frac{\Delta H_0+\Delta C_p \cdot (T-T_0)}{T(1+K)}\right]^2 \cdot K/R, \quad (1)$$

where

$$K=\exp\left[\frac{\Delta H_0-\Delta C_p \cdot T_0}{R}\left(\frac{1}{T_0}-\frac{1}{T}\right)+\frac{\Delta C_p}{R}\ln\frac{T}{T_0}\right]$$
$$R=\frac{8.31}{MW \cdot n}\ J/(g \cdot K). \quad (2)$$

Here, T is absolute temperature; $C_{p,D}$ is the specific heat capacity of the denatured protein linearly extrapolated to the transition region; ΔH_0, enthalpy of protein denaturation at mid-transition temperature T_0; ΔC_p, heat capacity change accompanying thermal denaturation. ΔH_0, ΔC_p, T_0 and n were used as the fitting parameters. The analogous expression for the model of two successive cooperative transitions [2] is:

$$C_p=(C_{p,N}+C_{p,I} \cdot K_1+C_{p,D} \cdot K_1 \cdot K_2)/(1+K_1+K_1 \cdot K_2)+$$
$$+\left[\frac{(1+K_2)\cdot\Delta H_1^2+2\cdot K_2\cdot\Delta H_1\cdot\Delta H_2+(1+K_1)\cdot K_2\cdot\Delta H_2^2}{T^2(1+K_1+K_1\cdot K_2)^2}\right] \cdot K_1/R$$
$$\Delta H_i=\Delta H_{0,i}+\Delta C_{p,i} \cdot (T-T_{0,i}), i=1,2 \quad (3)$$

$$K_i=\exp\left[\frac{\Delta H_{0,i}-\Delta C_{p,i} \cdot T_{0,i}}{R}\left(\frac{1}{T_{0,i}}-\frac{1}{T}\right)+\frac{\Delta C_{p,i}}{R}\ln\frac{T}{T_{0,i}}\right], i=1,2$$
$$R=\frac{8.31}{MW \cdot n}J/(g \cdot K), \quad (4)$$

where i values 1 and 2 correspond to the aforementioned parameters, characterizing the transitions between states I and N, D and I, respectively. Fitting parameters were $\Delta H_{0,i}$, $\Delta C_{p,i}$, $T_{0,i}$ and n.

The expression for free energy change in the simplest two-state thermal transition is:

$$\Delta G(T)=\Delta H_0 \cdot (1 - T/T_0)+\Delta C_p \cdot T \cdot [\, 1 - T_0/T - \ln(T/T_0)] \quad (5)$$

The uncertainties in determination of ΔH_0 and ΔC_p parameters may reach several percents. The lowest level of the parameter uncertainties is exemplified by studies of thermal denaturation of rat oncomodulin using confidence interval analysis [37], showing that uncertainties of T_0, ΔH_0 and ΔC_p parameters can be below ±0.2°C, ±0.5% and ±1%, respectively.

2.4. Circular dichroism

Circular dichroism (CD) measurements were carried out with a JASCO J-810 spectropolarimeter (JASCO, Japan), equipped with a Peltier-controlled cell holder. The instrument was calibrated with an aqueous solution of d-10-camphorsulfonic acid (JASCO) according to the manufacturer's instruction. Cuvettes with pathlengths of 10 and 1.00 mm were used for near- and far-UV regions, respectively. Protein concentrations were 130–220 μM and 6–9 μM for near- and far-UV region measurements, respectively. The small contribution of the buffer was subtracted from the experimental spectra. Temperature scans were performed at several wavelengths simultaneously in a stepwise manner, allowing the sample to equilibrate at each temperature. The average heating rate was 0.5°C/min. Band width was 2 nm, averaging time 8 s.

2.5. Fluorescence analyses

Fluorescence studies were performed on a Cary Eclipse spectrofluorimeter (Varian), equipped with a Peltier-controlled cell holder. Bis-ANS fluorescence was excited at 385 nm. Spectrofluorimetric temperature scans were performed stepwise allowing the sample to equilibrate at each temperature. The temperature was monitored directly inside the cuvette using Cary temperature probe (Varian). The average heating rate was 0.5°C/min.

2.6. Estimation of equilibrium Ca^{2+} association constants

The binding of Ca^{2+} ions to pike α-parvalbumin can be successfully described by the sequential Ca^{2+}-binding scheme [38]:

$$\begin{aligned} &\overset{K_1}{\text{Protein}+Ca^{2+} \leftrightarrow \text{Protein} \cdot Ca^{2+}} \\ &\overset{K_2}{\text{Protein} \cdot Ca^{2+}+Ca^{2+} \leftrightarrow Ca^{2+} \cdot \text{Protein} \cdot Ca^{2+},} \end{aligned} \quad [3]$$

where K_1 and K_2 are equilibrium Ca^{2+} binding constants for the two active EF-hands of parvalbumin.

The calcium affinity of parvalbumin was estimated from the spectrofluorimetric titration of the Ca^{2+}-free protein with a $CaCl_2$ standard, followed by a spectrofluorimetric titration of the Ca^{2+}-loaded protein with EDTA potassium salt at a fixed pH. Calculations of the Ca^{2+} association constants from the experimental data were performed after taking into account the competition between the protein and the chelator for Ca^{2+} ions, which is described by the scheme [3] with the addition of the equilibrium [4]:

$$\overset{K_{EDTA}}{\text{EDTA}+Ca^{2+} \leftrightarrow \text{EDTA} \cdot Ca^{2+}} \quad [4]$$

The Ca^{2+} association constant for EDTA, K_{EDTA}, was calculated according to Schwarzenbach and Flaschka [39]. The data were globally fitted using FluoTitr v.1.2 software [40]. The fit was achieved by variation of the binding constants K_1 and K_2. The quality of the fit was judged by the randomness of residuals distribution. The resulting accuracy of the Ca^{2+} binding constants was about ±1/4 orders of their magnitudes.

2.7. Predictions of intrinsic disorder

The predictions of the intrinsic disorder propensity of PAs were performed using the Various Short-Long, version 1 Predictor Of Natural Disordered Regions (PONDR®-VSL1), which is an ensemble of logistic regression models that predict per-residue order-disorder [41,42]. Predictor inputs include PSI-blast profiles [43], as well as PHD [44] and PSI-pred [45] secondary structure predictions.

2.8. Analysis of protein cavities

The coordinates of crystal structures of the Ca^{2+}-bound parvalbumins were obtained from the Protein Data Bank (http://www.rcsb.org/pdb/) [46]: entry code 1PVA (chain A) – pike α_2-PA [47]; 1RWY (chain A) – rat α- PA [48]; 1RRO – rat oncomodulin (β-PA) [49] and 4CPV – carp 4.25 PA [50]. All water molecules, acetyl groups, and ligands (except calcium atoms) were removed from the PDB files.

Structural cavities (interior empty spaces that are not accessible to the solvent probe) were calculated using CASTp online service (http://sts-fw.bioengr.uic.edu/castp/) [51]. The area and volume of each cavity was analytically calculated in molecular surface (Connolly's surface). A water molecule was used as the solvent probe. Figures were prepared using MolScript software [52].

3. Results

3.1. Thermal denaturation of calcium-loaded parvalbumins

The scanning microcalorimetry measurements of Ca^{2+}-loaded forms (1 mM $CaCl_2$) of five parvalbumins from different organisms (cod PA, α and β isoforms of pike and rat PAs) in a wide temperature range (15–125°C) revealed three protein groups (Figure 1), which qualitatively differ from each other by their thermal behavior. The first group included both parvalbumins from rat exhibiting a single heat-sorption peak. Analogous behavior was previously reported for parvalbumin III from mirror carp [53]. The second group included cod PA and pike α-PA, which unexpectedly showed two distinct heat-sorption peaks, not revealed so far for any representative of the PA family. Finally, pike β-PA exhibiting fairly complicated denaturation behavior represented the last group. It possessed a single distinct heat-sorption peak followed by a notable liberation of enthalpy at temperatures above 100°C, which may reflect the occurrence of the oligomerization process. The first peak corresponded to the peak found in the previous DSC study of this PA by Permyakov *et al.* [54], who did not reveal any evident processes with negative enthalpy change, possibly because of the narrower temperature range studied (50°C–105°C).

The thermodynamic analysis of the single heat-sorption peaks observed for Ca^{2+}-saturated rat parvalbumin isoforms α and β (Figure 1) according to the *cooperative two-state model* [1] (Figure 2a, Table 1) revealed that the cooperativity of the thermal transition, *n*, was less than 1. In fact, *n* equaled to 0.53 and 0.79 for isoforms α and β, respectively. It is important to note that *n* is equivalent to the ratio of van't Hoff enthalpy to calorimetric enthalpy ($\Delta H_{VH}/\Delta H_{cal}$), frequently used in thermodynamic analysis of thermal denaturation transitions. The *n* value being different from unity implied that the thermal denaturation of Ca^{2+}-bound rat parvalbumins did not obey the simple two-state ("all-or-none") mechanism, and the value being

below 1 was indicative of an intermediate state formation in the course of denaturation [55]. Similar analysis of a single heat-sorption peak observed for Ca^{2+}-loaded parvalbumin III of mirror carp also gave an *n* value below 0.9 [53], suggesting the complex mechanism of this transition.

The multistage character of the thermal denaturation of Ca^{2+}-loaded parvalbumins became apparent when the melting of pike α-PA and cod PA was analyzed. These proteins clearly exhibited two separate heat-sorption peaks separated by 20–30°C (Figure 1). Unfortunately, the DSC data for cod PA were complicated by aggregation (judged from the downward bend of the DSC curve at elevated temperatures). At the same time, the first (low-temperature) transition of pike α-PA was fully reversible (upon heating up to 98°C; data not shown), which made it suited for thermodynamic analysis. The analysis of this peak according to the *cooperative two-state model* gave n=0.93, which fall into the range of 0.93 to 0.98, typical for the "all-or-none" transitions [55]. Although the second (high-temperature) transition of pike α-PA was not reversible (data not shown), the full heat-sorption curve can nevertheless be adequately described by the *model of two successive cooperative transitions* with fixed n=1 (Figure 2b, Table 1), which implies that the full thermal denaturation process can be regarded as two sequential "all-or-none" type transitions. It should be noted that all thermodynamic parameters describing the first thermal transition were independent of the model employed ([1] or [2], fixed n=1; maximum $\Delta G(T)$ is 1.35 J/g (15.9 kJ/mol) at 45°C) because of the large distance (~30°C) between these transitions. Apparently, similar parameters of the second thermal transition represented some effective values because of its irreversibility.

The absence of evident protein association/dissociation processes in the course of the denaturation of pike α-PA was further confirmed by measurements of the dependence of the DSC heat-sorption curves upon protein concentration. The form of the first heat-sorption peak and the values of mid-temperatures of the both heat-sorption peaks did not change upon more than 3-fold increase in PA concentration from 0.7 to 2.6 mg/ml (10 mM $CaCl_2$; data not shown). Furthermore, SDS and native PAGE studies of pike α-PA samples heated to 130°C did not reveal the presence of protein oligomeric forms or fragments (data not shown).

It should be mentioned that several (at least four) thermal transitions were previously detected calorimetrically in the 80°C–115°C range for holo-form of pike α-PA under fairly peculiar conditions: a 20 mM parvalbumin solution with a scan rate of 20°C/min [56]. The authors suggested that they could correspond to the unfolding of the secondary structure elements. The manifestation of separate second heat-sorption peak was also reported for Ca^{2+}-loaded parvalbumin III of mirror carp, but the appearance of this effect required the decrease of pH down to 6 or lower [53]. In the case of pike α-PA, the lowering of pH down to 5.2 caused the approaching of the heat-sorption peaks to each other for about 13°C (mid-transition temperatures are 96°C and 111°C, for the first and second thermal transitions, respectively; data not shown). A similar experiment performed for rat β-PA did not reveal an appearance of any extra heat-sorption peaks (data not shown). Thus, the occurrence of an additional well-defined heat-sorption peak in Ca^{2+}-loaded parvalbumin was greatly dependent on its amino acid sequence and environmental conditions.

3.2. Structural features of the thermal denaturation intermediate of Ca^{2+}-bound pike α-PA

The changes accompanying the second thermal transition in pike α-PA ($t_{1/2}$=120.0°C; Figure 1, Figure 2b) started at temperatures above 100°C, which prevented the studies of this transition using conventional spectroscopic techniques (without additional pressurization of solution). Meanwhile, the same circumstance allowed ascribing any observable spectroscopic changes at temperatures below 100°C to the first thermal transition ($t_{1/2}$=90.5°C), which made it possible to characterize the intermediate spectroscopically. It is of interest to compare structural properties of this state with properties of the apo-PA lacking rigid tertiary structure [40].

The CD data shown in Figure 3a indicated that the first thermal transition in pike α-PA was accompanied by a decrease in absolute values of molar ellipticity ([θ]) at 222 nm (far-UV region) and 268 nm (near-UV), reflecting a loss of α-helical structure and the attainment of more symmetric and mobile environment of its aromatic residues (9 Phe), respectively. Extrapolation of the [θ] values to 100°C showed that the conversion of PA from the native to the intermediate state resulted in a decrease of the difference between [θ] values for the apo- (it lacks fixed tertiary structure) and Ca^{2+}-bound protein forms by about 20% and 27%, for far- and near-UV regions, respectively. Thus, the changes of helical content and symmetry and mobility of environment of Phe residues that occur in the first thermal transition were relatively limited, and the most drastic changes seem to occur in the second transition.

The ability of the hydrophobic probes ANS and bis-ANS to change their fluorescent properties upon association with exposed hydrophobic protein regions is widely used for detection of kinetic and equilibrium folding intermediates of proteins, which possess an increased (with respect to both native and fully denatured protein states) affinity to the probes (reviewed in [57]). The association of bis-ANS with Ca^{2+}-loaded pike α-PA at 30°C caused a characteristic blue shift (*ca* 15 nm; Figure 3b) of bis-ANS fluorescence spectrum (λ_{max}) and an increase in its relative fluorescence quantum yield (Q) for 50% (not shown). The same effects for apo-PA, exhibiting molten globule-like properties [40], were expectedly much more prominent: 43 nm blue shift of λ_{max} and 47-fold increase in Q value. The elevation of temperature up to 94°C was accompanied by continuous dissociation of bis-ANS molecules from apo-PA, as evidenced by the gradual red shift of bis-ANS fluorescence spectrum maximum (Figure 3b). The same behavior was observed for Ca^{2+}-bound PA up to *ca* 70°C, followed by a blue shift of bis-ANS fluorescence spectrum maximum. The latter process reflected the accumulation of the intermediate, possessing an elevated affinity to bis-ANS with respect to the native PA. Furthermore, at 94°C the magnitude of λ_{max} for Ca^{2+}-PA was lower than that for apo-protein by about 8 nm, which suggested the conservation of some ordered structure in the intermediate state compared to denatured apo-PA. Thus, the probing of Ca^{2+}-loaded PA using bis-ANS showed features characteristic for folding intermediates.

The solvent exposure of hydrophobic residues in the course of the first thermal transition, monitored by fluorescence of bis-ANS probe, was in accord with the pronounced heat capacity change accompanying the denaturation process (ΔC_p=0.49 J/(g*K)). Meanwhile, the resulting heat capacity of the intermediate was indistinguishable from that for the apo-form, which suggested a very high level solvation of the hydrophobic groups, inconsistent with the results of the near-UV CD and the presence of an additional thermal transition within PA molecule. This contradiction can be partially resolved assuming that the Phe residues of the intermediate remain involved into the most stable thermodynamic domain.

Since Ca^{2+} ions bound to pike PA were crucial for the maintenance of integrity of its tertiary structure [40], the partial loss of rigid tertiary structure in α-PA, which occurred in the first thermal transition, could be a consequence of the Ca^{2+} ion dissociation. The measurements of Ca^{2+} affinities of both active EF-hands of pike α-PA as a function of temperature (Figure 3c; using the model of sequential filling of Ca^{2+} binding sites [3]) revealed their strong decrease at elevated temperatures (*ca* 0.65 orders of magnitude per 10°C). Nevertheless, the values of Ca^{2+} association constants at 95°C ($K_1=2\times10^4$ M^{-1} and $K_2=1.1\times10^5$ M^{-1}) were still sufficiently high for efficient (>95%) filling of both sites in 1 mM $CaCl_2$. Thus, the intermediate PA state at 95°C was mostly Ca^{2+}-loaded, but further elevation of temperature may cause Ca^{2+} dissociation due to the strong temperature dependencies of K_1 and K_2. In this case, one can expect to see a shift of the second thermal transition toward higher temperatures upon an increase of Ca^{2+} concentration because of the filling of the fully denatured protein by Ca^{2+}. In fact, the increase in calcium concentration up to 10 mM (Figure 4c, Table 1) resulted in a shift of the second thermal transition toward higher temperatures by 2.0°C, while the first transition

was unaffected. This fact implied that the fully denatured state of the protein was not saturated by Ca^{2+} ions at 1 mM $CaCl_2$ concentration. Hence, the dissociation of Ca^{2+} ion(s) occurred in the second transition.It is important to note that the protein saturation with Ca^{2+} ions was not a prerequisite for the manifestation of the second thermal transition in pike α-PA. Two well-resolved heat-sorption peaks were observed for the protein with *ca* 2 Ca^{2+} ions bound per PA molecule. Furthermore, DSC measurements at calcium to protein molar ratios 1.5, 1, and 0.5 revealed that the decrease in the calcium content resulted in a gradual approaching of the heat-sorption peaks to each other, which showed that calcium binding was a key factor stabilizing the intermediate state (data not shown).

3.3. GdmCl-induced changes of the thermal transitions in pike α-parvalbumin

The DSC measurements on Ca^{2+}-bound pike α-PA in the presence of different concentrations of denaturant guanidinium chloride (25 mM to 1.6 M of GdmCl) revealed distinct differences in the sensitivities of the two thermal transitions to the GdmCl action (Figure 4). In the presence of 85 mM GdmCl, the first thermal transition was downshifted only by *ca* 4°C, whereas the second transition shifts toward the first transition by 10°C. The results of the thermodynamic analysis of the DSC data based upon the model of two successive cooperative transitions [2] are shown in Figure 4b. The increase in GdmCl concentration up to 250 mM resulted in a nearly complete overlapping of the transitions. A further increase in the GdmCl concentration was accompanied by a gradual shift of the single heatsorption peak toward the lower temperatures. The thermal denaturation at these conditions can be successfully described by the cooperative two-state model [1] with *n* lying in the range 0.31–0.73 (Figure 4b). In this sense, the thermal behavior of pike α-PA in the presence of high GdmCl concentrations resembled the melting of both Ca^{2+}-bound rat PAs in the absence of denaturant (*n*=0.53 and 0.79). Thus, GdmCl greatly affected the population of the thermal denaturation intermediate of pike α-PA.

The unexpectedly low resistance to the GdmCl action observed for the second thermal transition of pike α-PA can be easily rationalized in terms of the number of denaturant molecules bound per a molecule of PA upon protein denaturation (*X*). According to the denaturant binding model (see, for example, [58]), a protein molecule unfolds with an increasing denaturant concentration because more denaturant binding sites are exposed in the unfolded protein state than in the folded one. The relationship between the *X* value and the protein thermal transition sensitivity to denaturant action (dT_0/da_D, where T_0 is the mid-transition temperature and a_D is the activity of denaturant) can be easily derived from van't Hoff's law:

$$X = -(dT_0/da_D) \cdot a_D \cdot \Delta H_0/(RT_0^2).$$

The analysis of the DSC data obtained at the GdmCl concentrations of 25 mM and 85 mM (Figure 4a,b) according to this equation revealed about 2.0–2.2-fold excess in the *X* value for the second thermal transition (equals 1.9 at 85 mM GdmCl) over the *X* value for the first transition. Since the enthalpy of GdmCl binding to both folded and unfolded protein states is negative [59] (hence, the equilibrium GdmCl association constant decreases with temperature), the second transition was accompanied by the more prominent changes in the PA accessibility to the denaturant molecules. The conclusion was further supported by the CD data (Figure 3a), suggesting relatively small (20–27% of the expected overall denaturation effect) changes in PA helical content, and the symmetry and mobility of the environment of its Phe residues in the first thermal transition. At the same time, the heat capacity change in the first thermal transition was very high, suggesting a pronounced thermally-induced solvent exposure of PA hydrophobic groups. In all likelihood the difference in the *X* values for these transitions can be explained by the preferential binding of GdmCl molecules to the fully unfolded state.

Since the second thermal transition in pike α-PA was accompanied by the solvation of the negatively charged Ca^{2+}-binding carboxylates (see above), one could expect an increase in affinity of the protein to the positive GdmCl molecules. In this case, considering that the energetics of the charge-charge interactions in pike α-PA is governed by its Ca^{2+}-binding loops [40], the action of GdmCl on PA stability should be similar to the action of ionic strength. In fact, both GdmCl (at concentrations below 85 mM) and increased ionic strength influenced mainly the second thermal transition (Figure 4a and Figure 5b, respectively). The GdmCl-induced perturbations of the charge-charge interactions in the thermophilic esterases, causing an increased susceptibility to GdmCl, has been reported previously [60]. Here the same mechanism may be responsible for the unexpectedly low resistance of the second transition of pike α-PA to GdmCl.

It should be noted that the addition of GdmCl to pike α-PA switched the protein thermal behavior in such a way that the GdmCl-destabilized pike α-PA possessed thermal denaturation similar to that of rat PAs. The destabilizing action of GdmCl on the second thermal transition in pike α-PA was effectively reversed by means of a 10-fold increase in $CaCl_2$ concentration (Figure 4c, Table 1): in the presence of 85 mM GdmCl the addition of 10 mM $CaCl_2$ shifted the mid-transition temperature ($t_{1/2}$) of the second transition toward higher temperatures by 8.5°C ($t_{1/2}$ is *ca* 3°C lower than that at 10 mM $CaCl_2$ in the absence of GdmCl), whereas the first transition was virtually unaffected. Thus, the saturation of the EF-hands of PA with Ca^{2+} decreased the second thermal transition sensitivity to the GdmCl action. This effect can be regarded as a trivial consequence of Ca^{2+}-induced stabilization of protein structure, or as a competition between calcium ions and GdmCl molecules for the same binding sites. On the other hand, the selectivity of the observed effects with respect to the second thermal transition indicated that at least one of the Ca^{2+}-binding sites underwent structural rearrangement during this transition. Hence, the intermediate state realized between the two transitions was likely to be characterized by conserved CD or/and EF domain(s). The conclusion was in line with the observation that the intermediate state was Ca^{2+}-loaded in 1 mM $CaCl_2$ (Figure 3c). The increased stability of at least one of the PA Ca^{2+}-binding domains could be a reason for the appearance of an additional thermodynamic domain.

3.4. Thermal denaturation of magnesium- and sodium-loaded forms of pike α-parvalbumin

It was previously shown that metal-free forms of pike PAs are characterized by the absence of rigid tertiary structure [40]. In contrast to calcium ions, the binding of other physiologically significant ions, Mg^{2+} and Na^{+}, to pike α-PA resulted in the appearance of a single heat-sorption peak in DSC thermograms (Figure 5a). The stabilizing effect of magnesium binding was expectedly less pronounced when compared with that of calcium binding ($t_{1/2}$ is *ca* 77°C in 1 mM $MgCl_2$, compared with 90°C in 1 mM $CaCl_2$) and even less pronounced for Na^{+}-binding ($t_{1/2}$ is *ca* 33°C at 300 mM NaCl). Analogous thermal stability changes upon metal ions exchange were previously observed for other members of PA family (for review, see [8]). For instance, the $t_{1/2}$ value for pike β-PA was shown to decrease from *ca* 87°C to 67°C upon exchange of Ca^{2+} ions (1 mM $CaCl_2$) by Mg^{2+} (8 mM $MgCl_2$) [54].

In contrast to the Ca^{2+}-bound form, the thermal denaturation of both Mg^{2+}- and Na^{+}-loaded forms of pike α-PA was well described by the *cooperative two-state model* [1] with fixed n=1 (Figure 5a, Table 1). This suggested that melting of Mg^{2+}- and Na^{+}-forms of pike α-PA represented an “all-or-none” process. Hence, the exchange of Mg^{2+} by Ca^{2+} ions in the PA binding sites converted a simple “all-or-none” conformational transition into a more complex denaturation mechanism. Overall, the thermal denaturation mechanism of PA was fully controlled by the metal ions binding, and ranged from the absence of observable first-order transition to the complex mechanisms, involving at least one intermediate. The metal-binding proteins possessing this unique capability have not been reported so far, to the best of our

knowledge. One more peculiar feature of pike α-PA is that depending on its interactions with metal ions, it can be an intrinsically disordered protein (apo-form), an ordered protein of mesophilic (Na^+-bound state), thermophilic (Mg^{2+}-form), or even of the hyperthermophilic origin (Ca^{2+}-form).

It is well-known that remarkable conformational rearrangements have to occur in the EF-hand site of pike β-PA upon Ca^{2+}/Mg^{2+} exchange [47] to account for changes in the mode of metal ion coordination, as the coordination number decreased from seven oxygen atoms in the Ca^{2+}-loaded form to six oxygen atoms in the Mg^{2+}-loaded form. As a result, Glu101 at the relative position 12 in the EF-hand loop sequence (gateway 'Glu12') was shown to act as a bidentate ligand in the Ca^{2+}-loaded form and as a monodentate ligand in the Mg^{2+}-loaded form. In the CD site of PA, the homologous residue Glu62 displayed a behavior similar to that of Glu101 upon Ca^{2+}/Mg^{2+} exchange, based on NMR and FTIR evidence [61,62].

The complexity of the mechanism of thermal denaturation of metal-bound pike α-PA clearly correlated with the affinity of the protein to metal ions: the higher the affinity, the more complex mechanism was realized. Evidently, the metal-induced increase in the free energy of the PA denaturation ($\delta\Delta G_{Me}$) caused the gradual increase in the mid-transition temperature upon binding of Na^+ ions and exchange of Na^+ for Mg^{2+}. However, further increase of $\delta\Delta G_{Me}$ upon Ca^{2+} association resulted in a qualitative change of protein thermal behavior. Notably, a further increase of $\delta\Delta G_{Me}$ by means of substitution of Ca^{2+} in the binding sites by Tb^{3+} did not change the mechanism of denaturation (data not shown). This conformational switch seemed to be triggered via the Ca^{2+}-induced stabilization of at least one of the active EF-hand domains of the intermediate. In this case, the population of the intermediate state should correlate with the calcium affinity of PA. This hypothesis was supported both by DSC measurements of Ca^{2+}-loaded pike α-PA in excess of KCl (Figure 5b), and by comparison of calcium affinities of pike and rat PAs. The electrostatic screening of charge-charge interactions within calcium-binding sites of pike α-PA [40] caused by the addition of 1 M KCl resulted in the lowering of the distance between the thermal transitions by 11°C (Table 1). Both Ca^{2+} association constants (K_1 and K_2) for pike α-PA exceeded those for rat α-isoform, especially K_2 (by an order of magnitude) [25]. For this reason, higher population of the intermediate can be expected for pike protein. In fact, the formation of the intermediate state was evidently observed for Ca^{2+}-loaded pike α-PA (Figure 1 and Figure 2b), whereas the existence of intermediate(s) in the case of the rat protein can be established only upon a detailed thermodynamic analysis of DSC data (n=0.53, model [1]). Similarly, the Ca^{2+}-binding constants K_1 and K_2 for rat α-PA exceeded those for β-isoform by 1 and 1.5 orders of magnitude, respectively. Therefore, the n value (being a measure of population of the intermediate state(s) in the course of denaturation) is much closer to 1 for β-isoform (0.79 versus 0.53 for α-PA). Therefore, the higher the Ca^{2+} affinity of PA, the higher population of the intermediate in the course of thermal denaturation can be expected.

3.5. Structural determinants of the thermal denaturation intermediate of Ca^{2+}-bound pike α-PA

Similar to other representatives of PA family, pike α-PA was characterized by extensive pair-wise interactions of all subdomains (AB, CD, and EF) (Figure 6), which prevented from obvious assignment of separate structural subdomain(s) to the thermodynamic domains. The quantitative estimate of probability of the individual protein residues to be included into fixed tertiary structure can be achieved via the so-called PONDR score. The scores for various PAs were assessed on the per-residue basis using the PA amino acid sequences and a computational tool for the per-residue protein order-disorder prediction (Predictors Of Natural Disordered Regions, PONDR; see www.disprot.org/predictors.php). The lower the PONDR score of a

specific residue, the higher the probability of its inclusion into fixed tertiary structure of the protein.

The appearance of an additional heat-sorption peak in some representatives of PA family ("group 2", which includes pike α-PA and cod PA) is a consequence of stabilization of the intermediate state compared with PAs exhibiting single heat-sorption peak in the Ca^{2+}-bound form (proteins of group 1, which includes carp [53] and rat PAs). The stabilized regions of the intermediate were expected to possess a relatively higher order propensity. Therefore, the regions of polypeptide chains of proteins from group 2, whose PONDR scores were lower than those of the group 1 PAs, were suggested to correspond to the ordered regions preserved in the intermediate state, and, respectively, were suggested to constitute the most stable of the thermodynamic domains.

The ranges of possible PONDR score values for PAs of groups 1 and 2, estimated by means of the well-established predictor of protein disorder PONDR®-VSL1 [41,42], are shown in Figure 6a. The PONDR analysis revealed two distant sequence regions for PAs from group 2, possessing PONDR scores essentially lower than those for the group 1: residues 34–40 (7 residues long) and 81–105 (25 residues). The longer region belonged to the EF subdomain (residues 76–108) and comprised the EF-hand loop 89–100, whereas the shorter region was located in the loop region between AB and CD domains. Although both regions identified by PONDR analysis were separated by 40 amino acids, an examination of their spatial location (Figures 6b,c) showed that they were involved in a direct contact via the residues L34 and A39 provided by the first region. The involvement of the EF-loop into the region likely to be preserved in the intermediate state is in line with the conclusion derived from experimental studies of pike α-PA that at least one of the Ca^{2+}-binding domains seems to be conserved in the intermediate.

Importantly, the average PONDR scores for the regions 34–40 and 81–105 of group 2 PAs were very close to 0.5 (0.48 and 0.56, respectively), the value corresponding to the boundary between ordered and disordered conformations. This suggested that these regions of PA *per se* cannot confer the expressed thermal stability to the protein. In fact, the PONDR algorithm was developed upon a consideration of the amino acid sequence alone, and did not take into consideration the effects potentially induced by the ligand binding. Calcium association profoundly stabilized PA structure due to the compensation of highly unfavorable charge-charge interactions of carboxylic groups within EF-hands of the protein [40]. At the same time, the average PONDR score for whole pike α-PA sequence was 0.54, which shows its overall instability. Thus, the binding of Ca^{2+} ion(s) was a prerequisite for appearance of hyperthermostable intermediate in the course of thermal denaturation of pike α-PA. In fact, the Ca^{2+} affinity measurements (Figure 3c) showed that the intermediate was Ca^{2+}-loaded in the presence of 1 mM $CaCl_2$.

While the Ca^{2+}-binding may confer stability to CD and EF domains of PA, the electrostatically inactive AB domain of pike α-PA [40] was intrinsically unstable (an average PONDR score is 0.55±0.11), which suggested the possible disorganization of this subdomain in the course of the first thermal transition. Therefore, the PONDR analysis showed that the thermal intermediate of pike α-PA was likely to be characterized by the disordered AB subdomain and the preserved EF subdomain. It should be mentioned that the average PONDR scores for the CD and EF subdomains of pike α-PA are 0.47±0.05 and 0.61±0.05, respectively, which suggested lower intrinsic stability of the EF domain. However, the higher Ca^{2+}-induced stability increase can compensate the lower stability of the EF domain alone. In fact, taking into account the sequential mechanism of the filling of PA Ca^{2+}-binding loops (scheme [3]) and the suggestion that the CD site was filled by Ca^{2+} first (reviewed in [8]), it can be concluded

that, at temperatures above 40°C, the effective calcium affinity of the EF site in pike α-PA was higher than that of the CD site by about an order of magnitude (Figure 3c).

One of the approaches which allows the discovery of the sites of loosened interactions between protein residues is an examination of protein cavities (interior empty spaces that are not accessible to the solvent probe). The results of comparative analysis of the locations of the cavities within X-ray structures of four PAs belonging to both groups 1 and 2 using CASTp server [51] are shown in Table 2. Evidently, pike α-PA (cod PA is excluded, since its tertiary structure is unknown) was notably different from three other PAs analyzed: it contained 9 cavities versus 4–6 in other PAs. Furthermore, the total area (*S*) and volume (*V*) of the cavities in pike α-PA exceed the *S* and *V* values evaluated for other PAs by more than 40% (Table 2). Hence, the overall packing density of pike α-PA was lower than that of other PAs. The *V* value of all cavities of pike α-PA corresponded to about 1.5% of the total molecule volume (estimated according to Hackel *et al.* [35]), which was comparable with the experimental estimates of specific volume changes accompanying protein unfolding (see, for example, [63]).

The energetic penalty for the increase in the total volume of cavities within pike α-PA by about 91 $Å^3$ (with respect to the average *V* value for all PAs in group 1) can be estimated from the known average change in free energy of unfolding for deletion of one methylene group from hydrophobic core ($V \approx 27$ $Å^3$; −1.3±0.5 kcal/mol [64]):

$$\Delta\Delta G_p \approx -4.4 \pm 2 \text{ kcal/mol (it corresponds to ca 3.4 methylene groups).}$$

At the same time, the difference between changes in free energy of unfolding, accompanying two thermal transitions of Ca^{2+}-bound pike α-PA, $\Delta G_i(T)$ (i=1,2), can be estimated from the free energy change of the first transition, $\Delta G_1(T)$ (Equation (5)):

$$\Delta\Delta G_{1\to 2}=\Delta G_2(T) - \Delta G_1(T) \approx -\Delta G_1(T_{0,2})=6.7 \text{ kcal/mol},$$

where $T_{0,2}$ is a mid-transition temperature for the second transition.

The proximity of the absolute values of $\Delta\Delta G_p$ and $\Delta\Delta G_{1\to 2}$ suggested that the energetic difference between the two thermal transitions observed for pike α-PA can be successfully compensated by the energy related to the increased volume of its cavities. Therefore, the cavities of pike α-PA were likely to be the major factor determining the disturbance of structural cooperativity (interactions between subdomains) within pike α-PA. The Ca^{2+}-bound forms of PAs of group 1, displaying the single but complex heat-sorption peak, may also contain two thermodynamic domains but with similar stabilities.

The analysis of the location of cavities within different PAs shows that they are mostly limited to the interfaces between subdomains AB, CD, and EF. To compare the cavities belonging to different subdomain interfaces the *S* and *V* values for the following non-intersecting sets of cavities were estimated (Table 2):

1. Central cavities, formed by atoms provided by at least three out of four helices C, D, E, and F;
2. Cavities formed by atoms provided by either D and E helices, including DE loop, or C and F helices (“peripheral cavities”);
3. Cavities formed by atoms provided by B and D helices.

The combination of the two first groups of cavities characterized the interface between the Ca^{2+}-binding CD and EF domains (the cavity-forming atoms for pike α-PA are shown in Figures 6b,c).

The *S* and *V* values for the central cavities in pike α-PA (which correspond to about half of the total values) were more than 2.5- and 1.9-fold higher than the analogous values for other PAs, respectively. The same values for the peripheral cavities of pike α-PA exceeded those for other PAs by more than 20%. Overall, the interface between CD and EF subdomains of pike α-PA was much more loosely packed in comparison with other PAs considered. At the same time, the parameters of cavities formed by the pike α-PA B and D helices (Table 2) were comparable with those for other PAs. Interestingly, the number of residues of AB domain and BC loop (residues 1–38/39) involved in the formation of the cavities was 10 for pike α-PA versus 4 for carp protein and 3 for both rat PAs. This was due to the presence of an additional cavity located between helices A and B of the pike protein ($S = 26$ Å^2 and $V = 12.5$ Å^3). Thus, the cavity analysis indicated that this part of a protein molecule was somewhat less tightly packed in pike α-PA compared with the other PAs. Nevertheless, the cavities located at the interface between CD and EF domains comprised about 85% of the area and volume of all cavities within pike α-PA. This implied that the contribution of the AB domain into the cavity formation was relatively limited.

The multiple cavities spread between the EF and CD subdomains of pike α-PA (Figures 6b,c) were likely to impair the stabilizing interactions between these subdomains, resulting in a loss of structural cooperativity. The interface between EF and CD domains possibly served as a boundary between the two thermodynamic domains of the protein. The PONDR analysis suggested that the most stable of the thermodynamic domains likely contained EF subdomain, whereas CD and AB subdomains were involved in the least stable thermodynamic domain. Therefore, the intermediate state was likely to retain the tertiary structure of the EF subdomain, whereas CD and AB subdomains were likely unfolded in this state. Despite the loss of the rigid tertiary structure of one of the Ca^{2+}-binding subdomains in the intermediate state, both pike α-PA sites preserved some Ca^{2+}-binding ability being occupied at 95°C in 1 mM $CaCl_2$ (see above; Figure 3c).

The available literature data further supported the conclusion on the disturbance of the structural cooperativity between CD and EF subdomains in pike α-PA. On the other hand, both rat PAs demonstrated the concerted changes of calcium affinity, which suggested the cooperative behavior of these subdomains (summarized in [25]). The calcium affinities (K_1 and K_2) of AB/CD-EF complexes (associated AB and CD-EF fragments) of both rat PAs were lowered by *ca* 2 orders of magnitude for both Ca^{2+}-binding sites. A different situation was observed for pike α-PA: while K_1 of AB/CD-EF complex was decreased by an order of magnitude, K_2 remained virtually unaffected.

4. Discussion

Small globular proteins with rigid tertiary structure typically exhibit a single-step thermal denaturation transition. Therefore, the complex multistage process observed for Ca^{2+}-bound parvalbumin, lacking an obvious domain structure, was rather unexpected. The rare examples of similar denaturation behavior include DNA binding domains (DBDs) of sequence-specific and non-sequencespecific HMG box proteins (Mr *ca* 10 kDa; all α class) (reviewed in [3]), and some of calcium-binding lysozymes (Mr *ca* 14 kDa; (α+β) class) (reviewed in [4]) Meanwhile, the known cases of manifestation of complex thermal denaturation of small globular proteins are accompanied by at least one low-temperature (low enthalpy) transition. As a consequence, some of these proteins are partially unfolded at the lowest accessible

temperatures [65]. The markedly different situation is observed for highly stable Ca^{2+}-loaded PA, having only high-temperature transitions.

Our experimental and computational data clearly showed that the “empty” EF-hands of pike α-PA in the absence of metal cations were intrinsically disordered because of the energetically unfavorable presence of multiple carboxylic groups within the Ca^{2+}-binding loops, whereas the metal-induced energy gain caused the profound stabilization of the EF-hands resulting in some cases in hyperstable structures, which denatured at temperatures as high as 120°C. The extreme thermal stability was previously reported for another representative of the EF-hand protein family, timothy grass allergen, Phl p 7, the Ca^{2+}-bound state of which denatured at temperatures above 120°C [66]. Pike α-PA is a unique protein, since it demonstrated the most dramatic calcium-induced changes in thermal stability, to the best of our knowledge. It can be considered as an intrinsically disordered protein in apo-form (no detectable cooperative transition), an ordered protein of the mesophilic origin (in the Na^{+}-bound state, $t_{1/2}$ was *ca* 33° C at 300 mM NaCl), an ordered thermophilic protein (in the Mg^{2+}-bound state, $t_{1/2}$ was *ca* 77° C at 1 mM $MgCl_2$), or a hyperthermophilic protein (in the Ca^{2+}-loaded state, $t_{1/2}$ were *ca* 90° C and 120°C in 1 mM $CaCl_2$).

An even more impressive feature of pike α-PA not reported for any other metal-binding proteins was its ability to alter the mechanism of thermal denaturation depending upon the cation bound. While Na^{+} and Mg^{2+} loaded forms obeyed the simplest two-state unfolding model, characteristic for small globular proteins, the Ca^{2+}-bound form exhibited two distinct sequential transitions of the “all-or-none” type, evidencing the presence of two thermodynamic domains. Other PAs studied also demonstrated the complex mechanism of thermal denaturation in the Ca^{2+}-bound state, but the overlapping of contributing transitions did not allow any conclusions to be drawn concerning the exact mechanisms underlying the process. One could assume that, similarly to pike α-PA, these PAs possessed two thermodynamic domains, which, in contrast to the pike protein, had very close thermal stabilities.

Different lines of experimental evidences led to the conclusion that the intermediate state appearing in the course of the thermal denaturation of Ca^{2+}-loaded pike α-PA was stabilized by the bound calcium ions. Furthermore, an examination of the isolated cavities in different PAs showed that the manifestation of an additional thermodynamic domain within pike protein became possible due to the significantly decreased packing density of the interfaces between the Ca^{2+}-binding domains of the protein. The PONDR analysis of several PAs showed that the EF-subdomain and nearby BC loop were intrinsically stabilized in PAs exhibiting two heat-sorption peaks. Hence, both fragments were likely to be largely preserved in the intermediate states of these PAs. On the contrary, the intrinsically unstable AB domain, not stabilized by calcium ions, was likely to be melted in the course of the first thermal transition. Apparently, further residue-specific structural studies are required for elucidation of structural factors stabilizing the intermediate state.

It is of interest that the presence and the approximate location of two thermodynamic domains within PA structure could be predicted based on the recent observation that there was a considerable overlapping between the location of folding nuclei and the location of the so-called “root structural motifs” [67], which had unique overall folds and handedness [68]. PA structure included the only type of root structural motifs, α-α corner formed by the two consecutive α-helices, which were packed approximately crosswise and arranged into left superhelix. Each of the EF and CD subdomains of PA represented a separate α-α corner, and therefore should correspond to two different folding nuclei. Although the presence of two folding nuclei does not necessarily imply that the protein will possess two thermodynamic domains, this could take place under the conditions of loosened interactions between the two subdomains.

The presence of multiple thermodynamic domains within small globular proteins has been reported earlier (see above). Actually, the minimal size of thermodynamic domain can be as small as 20 residues, as exemplified by studies of Trp-Cage, a 20 residue miniprotein [69]. Despite a marginal stability, Trp-Cage possessed a distinct DSC heat-sorption peak. The example of parvalbumin showed that the additional thermodynamic domain may arise not only due to excessive protein size, but also due to ligand-induced stabilization of the intermediate state. In this sense, the thermodynamic domains of PA were not an intrinsic property of its polypeptide chain, but represented a consequence of the ligand-binding ability of the protein.

Parvalbumin, a soluble relaxing factor of fast muscles, is known to switch between Mg^{2+}-loaded and Ca^{2+}-loaded states. We show that these PA states were different from the viewpoint of structural cooperativity of the two thermodynamic domains, which was clearly seen upon thermal denaturation. Meanwhile, it is unknown whether or not the Ca^{2+}/Mg^{2+}-switch of structural cooperativity of thermodynamic domains of PA can manifest itself under physiologically relevant conditions. This feature of PA could be profitable for association with some unknown target(s). Recent experimental data (discussed in [28,70]) favor the conception that at least some of the representatives of PA family may be involved in target recognition and hence cannot be considered as “pure” metal-buffers.

There exists one more physiologically important aspect of the presented observations. As one of the major animal allergens [15] and a major allergen in various fish species [16], parvalbumin loses its allergenicity upon fish canning (exemplified by studies of tuna and salmon [71]), being resistant to conventional cooking. Since the temperature during industrial canning reaches 120° C, one can easily rationalize these observations based upon the data presented for pike α-PA (Figure 1, Figure 2b). The loss of PA allergenicity upon heating up to 120°C could be due to a non-reversible denaturation in the course of the second thermal transition, while cooking at 100°C should cause only a reversible denaturation of PA. It should be noted that this explanation is not satisfactory for the most recognized fish allergen, cod PA (Figure 1), due to its relatively low thermal stability. Meanwhile, the presence of natural osmolytes may confer the thermal stability, sufficient for resistance to heating up to 100°C.

The abbreviations used are

PA, parvalbumin
α-PA, α isoform of parvalbumin
β-PA, β isoform of parvalbumin
HEPES, N-(2-hydroxyethyl)piperazine-N’-(2-ethanesulfonic acid)
bis-ANS, 4,4’-dianilino-1,1’-binaphthyl-5,5’-disulfonic acid
EDTA, ethylenediaminetetraacetic acid
GdmCl, guanidinium chloride
SDS-PAGE, sodium dodecyl sulfate polyacrylamide gel electrophoresis
DSC, differential scanning calorimetry
CD, circular dichroism
PONDR, predictor of naturally disordered regions

Acknowledgements

We are indebted to Prof. Michael T. Henzl (University of Missouri) for providing the plasmids encoding rat parvalbumins. This work was supported in part by grants from the Program of the Russian Academy of Sciences «Molecular and Cellular Biology» (E.A.P.), Stiftelsens för Åbo Akademi forskningsinstitut (A.I.D.) and the Sigrid Jusélius Foundation (A.I.D.), R01 LM007688-01A1 (V.N.U.) and GM071714-01A2 (V.N.U.) from the National Institutes of Health. The support of the IUPUI Signature Centers Initiative is gratefully acknowledged.

References

1. Dumoulin M, Canet D, Last AM, Pardon E, Archer DB, Muyldermans S, Wyns L, Matagne A, Robinson CV, Redfield C, Dobson CM. Reduced global cooperativity is a common feature underlying the amyloidogenicity of pathogenic lysozyme mutations. J Mol Biol 2005;346:773–788. [PubMed: 15713462]
2. Jackson SE. How do small single-domain proteins fold? Fold Des 1998;3:R81–R91. [PubMed: 9710577]
3. Privalov PL, Dragan AI. Microcalorimetry of biological macromolecules. Biophys Chem 2007;126:16–24. [PubMed: 16781052]
4. Morozova-Roche LA. Equine lysozyme: the molecular basis of folding, self-assembly and innate amyloid toxicity. FEBS Lett 2007;581:2587–2592. [PubMed: 17531977]
5. Berchtold MW. Structure and expression of genes encoding the three-domain Ca2+-binding proteins parvalbumin and oncomodulin. Biochim Biophys Acta 1989;1009:201–215. [PubMed: 2688747]
6. Pauls TL, Cox JA, Berchtold MW. The Ca2+(−)binding proteins parvalbumin and oncomodulin and their genes: new structural and functional findings. Biochim Biophys Acta 1996;1306:39–54. [PubMed: 8611623]
7. Berchtold MW, Brinkmeier H, Muntener M. Calcium ion in skeletal muscle: its crucial role for muscle function, plasticity, and disease. Physiol Rev 2000;80:1215–1265. [PubMed: 10893434]
8. Permyakov, EA. Parvalbumin. New York: Nova Science Publishers; 2006.
9. Heizmann CW, Berchtold MW, Rowlerson AM. Correlation of parvalbumin concentration with relaxation speed in mammalian muscles. Proc Natl Acad Sci U S A 1982;79:7243–7247. [PubMed: 6961404]
10. Hackney CM, Mahendrasingam S, Penn A, Fettiplace R. The concentrations of calcium buffering proteins in mammalian cochlear hair cells. J Neurosci 2005;25:7867–7875. [PubMed: 16120789]
11. Berchtold MW, Means AR. The Ca2+-binding protein parvalbumin: molecular cloning and developmental regulation of mRNA abundance. Proc Natl Acad Sci U S A 1985;82:1414–1418. [PubMed: 3856270]
12. Muntener M, Kaser L, Weber J, Berchtold MW. Increase of skeletal muscle relaxation speed by direct injection of parvalbumin cDNA. Proc Natl Acad Sci U S A 1995;92:6504–6508. [PubMed: 7604022]
13. Schwaller B, Dick J, Dhoot G, Carroll S, Vrbova G, Nicotera P, Pette D, Wyss A, Bluethmann H, Hunziker W, Celio MR. Prolonged contraction-relaxation cycle of fast-twitch muscles in parvalbumin knockout mice. Am J Physiol 1999;276:C395–C403. [PubMed: 9950767]
14. Heizmann CW. Calcium signaling in the brain. Acta Neurobiol Exp (Wars) 1993;53:15–23. [PubMed: 8317243]
15. Jenkins JA, Breiteneder H, Mills EN. Evolutionary distance from human homologs reflects allergenicity of animal food proteins. J Allergy Clin Immunol 2007;120:1399–1405. [PubMed: 17935767]
16. Elsayed S, Bennich H. The primary structure of allergen M from cod. Scand.J.Immunol 1975;4:203–208. [PubMed: 1145128]
17. Bugajska-Schretter A, Elfman L, Fuchs T, Kapiotis S, Rumpold H, Valenta R, Spitzauer S. Parvalbumin, a cross-reactive fish allergen, contains IgE-binding epitopes sensitive to periodate treatment and Ca2+ depletion. J Allergy Clin Immunol 1998;101:67–74. [PubMed: 9449503]
18. Aas K, Elsayed SM. Characterization of a major allergen (cod). Effect of enzymic hydrolysis on the allergenic activity. J Allergy 1969;44:333–343. [PubMed: 4983319]
19. Elsayed S, Aas K. Characterization of a major allergen (cod). Observations on effect of denaturation on the allergenic activity. J Allergy 1971;47:283–291. [PubMed: 5280452]
20. Goodman M, Pechere JF. The evolution of muscular parvalbumins investigated by the maximum parsimony method. J Mol Evol 1977;9:131–158. [PubMed: 864720]
21. Kretsinger RH. Structure and evolution of calcium-modulated proteins. CRC Crit Rev Biochem 1980;8:119–174. [PubMed: 6105043]
22. Huriaux F, Vandewalle P, Focant B. Immunological study of muscle parvalbumin isotypes in three African catfish during development. Comp Biochem Physiol B Biochem Mol Biol 2002;132:579–584. [PubMed: 12091103]

23. Focant B, Vandewalle P, Huriaux F. Expression of myofibrillar proteins and parvalbumin isoforms during the development of a flatfish, the common sole Solea solea: comparison with the turbot Scophthalmus maximus. Comp Biochem Physiol B Biochem Mol Biol 2003;135:493–502. [PubMed: 12831769]
24. Permyakov EA, Medvedkin VN, Mitin YV, Kretsinger RH. Noncovalent complex between domain AB and domains CD*EF of parvalbumin. Biochim.Biophys.Acta 1991;1076:67–70. [PubMed: 1898866]
25. Henzl MT, Agah S, Larson JD. Association of the AB and CD-EF domains from rat alpha- and beta-parvalbumin. Biochemistry 2004;43:10906–10917. [PubMed: 15323551]
26. Rao KS, Gerday C. Low molecular weight proteins of pike (Esox lucius) white muscles. I. Extraction and purification-polymorphism. Comp Biochem.Physiol B 1973;44:931–937. [PubMed: 4709987]
27. Haiech J, Derancourt J, Pechere JF, Demaille JG. A new large-scale purification procedure for muscular parvalbumins. Biochimie 1979;61:583–587. [PubMed: 315239]
28. Permyakov SE, Karnoup AS, Bakunts AG, Permyakov EA. Sequence microheterogeneity of parvalbumin pI 5.0 of pike: a mass spectrometric study. Biochim Biophys Acta 2009;1794:129–136. [PubMed: 18930845]
29. Henzl MT, Graham JS. Conformational stabilities of the rat alpha- and beta-parvalbumins. FEBS Lett 1999;442:241–245. [PubMed: 9929009]
30. Rao KS, Gerday C. Low molecular weight proteins of pike (esox lucius) white muscles. II. Chemical and physical properties. Comp Biochem.Physiol B 1973;44:1113–1125. [PubMed: 4736651]
31. Pace CN, Vajdos F, Fee L, Grimsley G, Gray T. How to measure and predict the molar absorption coefficient of a protein. Protein Sci 1995;4:2411–2423. [PubMed: 8563639]
32. Henzl MT, Larson JD, Agah S. Influence of monovalent cations on rat alpha- and beta-parvalbumin stabilities. Biochemistry 2000;39:5859–5867. [PubMed: 10801337]
33. Blum HE, Lehky P, Kohler L, Stein EA, Fischer EH. Comparative properties of vertebrate parvalbumins. J.Biol.Chem 1977;252:2834–2838. [PubMed: 856805]
34. Privalov PL, Potekhin SA. Scanning microcalorimetry in studying temperature-induced changes in proteins. Methods Enzymol 1986;131:4–51. [PubMed: 3773768]
35. Hackel M, Hinz HJ, Hedwig GR. Partial molar volumes of proteins: amino acid side-chain contributions derived from the partial molar volumes of some tripeptides over the temperature range 10–90 degrees C. Biophys.Chem 1999;82:35–50. [PubMed: 17030339]
36. Makhatadze GI, Privalov PL. Heat capacity of proteins. I. Partial molar heat capacity of individual amino acid residues in aqueous solution: hydration effect. J.Mol.Biol 1990;213:375–384. [PubMed: 2342113]
37. Henzl MT, Davis ME, Tan A. Leucine 85 is an important determinant of divalent ion affinity in rat beta-parvalbumin (Oncomodulin). Biochemistry 2008;47:13635–13646. [PubMed: 19075559]
38. Permyakov EA, Medvedkin VN, Kalinichenko LP, Burstein EA. Comparative study of physiochemical properties of two pike parvalbumins by means of their intrinsic tyrosyl and phenylalanyl fluorescence. Arch.Biochem.Biophys 1983;227:9–20. [PubMed: 6639084]
39. Schwarzenbach, G.; Flaschka, H. Die komplexometrische titration. Stuttgart: Ferdinand Enke Verlag; 1965.
40. Permyakov SE, Bakunts AG, Denesyuk AI, Knyazeva EL, Uversky VN, Permyakov EA. Apo-parvalbumin as an intrinsically disordered protein. Proteins 2008;72:822–836. [PubMed: 18260106]
41. Peng K, Vucetic S, Radivojac P, Brown CJ, Dunker AK, Obradovic Z. Optimizing long intrinsic disorder predictors with protein evolutionary information. J Bioinform Comput Biol 2005;3:35–60. [PubMed: 15751111]
42. Obradovic Z, Peng K, Vucetic S, Radivojac P, Dunker AK. Exploiting heterogeneous sequence properties improves prediction of protein disorder. Proteins 2005;61:176–182. [PubMed: 16187360]
43. Altschul SF, Madden TL, Schaffer AA, Zhang J, Zhang Z, Miller W, Lipman DJ. Gapped BLAST and PSI-BLAST: a new generation of protein database search programs. Nucleic Acids Res 1997;25:3389–3402. [PubMed: 9254694]
44. Rost B, Sander C, Schneider R. PHD--an automatic mail server for protein secondary structure prediction. Comput Appl Biosci 1994;10:53–60. [PubMed: 8193956]

45. Jones DT, Ward JJ. Prediction of disordered regions in proteins from position specific score matrices. Proteins 2003;53:573–578. [PubMed: 14579348]
46. Berman HM, Westbrook J, Feng Z, Gilliland G, Bhat TN, Weissig H, Shindyalov IN, Bourne PE. The Protein Data Bank. Nucleic Acids Res 2000;28:235–242. [PubMed: 10592235]
47. Declercq JP, Tinant B, Parello J, Rambaud J. Ionic interactions with parvalbumins. Crystal structure determination of pike 4.10 parvalbumin in four different ionic environments. J Mol Biol 1991;220:1017–1039. [PubMed: 1880797]
48. Bottoms CA, Schuermann JP, Agah S, Henzl MT, Tanner JJ. Crystal structure of rat alpha-parvalbumin at 1.05 Angstrom resolution. Protein Sci 2004;13:1724–1734. [PubMed: 15169955]
49. Ahmed FR, Rose DR, Evans SV, Pippy ME, To R. Refinement of recombinant oncomodulin at 1.30 A resolution. J Mol Biol 1993;230:1216–1224. [PubMed: 8487302]
50. Kumar VD, Lee L, Edwards BF. Refined crystal structure of calcium-liganded carp parvalbumin 4.25 at 1.5-A resolution. Biochemistry 1990;29:1404–1412. [PubMed: 2334704]
51. Dundas J, Ouyang Z, Tseng J, Binkowski A, Turpaz Y, Liang J. CASTp: computed atlas of surface topography of proteins with structural and topographical mapping of functionally annotated residues. Nucleic Acids Res 2006;34:W116–W118. [PubMed: 16844972]
52. Kraulis PJ. MOLSCRIPT: a program to produce both detailed and schematic plots of protein structures. Appl.Crystallogr 1991;24:945–949.
53. Filimonov VV, Pfeil W, Tsalkova TN, Privalov PL. Thermodynamic investigations of proteins. IV. Calcium binding protein parvalbumin. Biophys.Chem 1978;8:117–122. [PubMed: 27259]
54. Permyakov EA, Kreimer DI, Kalinichenko LP, Shnyrov VL. Interactions of calcium binding proteins, parvalbumin and alpha-lactalbumin, with dipalmitoylphosphatidylcholine vesicles. Gen.Physiol Biophys 1988;7:95–107. [PubMed: 3396853]
55. Privalov PL. Stability of proteins: small globular proteins. Adv Protein Chem 1979;33:167–241. [PubMed: 44431]
56. Zanotti JM, Bellissent-Funel MC, Parello J. Hydration-coupled dynamics in proteins studied by neutron scattering and NMR: the case of the typical EF-hand calcium-binding parvalbumin. Biophys J 1999;76:2390–2411. [PubMed: 10233057]
57. Daughdrill, GW.; Pielak, GJ.; Uversky, VN.; Cortese, MS.; Dunker, AK. Natively Disordered Proteins. In: JK Buchner, T., editor. Protein Folding Handbook. Vol. Vol. I. KGaA, Weinheim, Germany: Wiley-VCH Verlag GmbH & Co; 2005. p. 275-357.
58. Aune KC, Tanford C. Thermodynamics of the denaturation of lysozyme by guanidine hydrochloride. II. Dependence on denaturant concentration at 25 degrees. Biochemistry 1969;8:4586–4590. [PubMed: 5353115]
59. Makhatadze GI, Privalov PL. Protein interactions with urea and guanidinium chloride. A calorimetric study. J Mol Biol 1992;226:491–505. [PubMed: 1322462]
60. Del Vecchio P, Graziano G, Granata V, Barone G, Mandrich L, Rossi M, Manco G. Denaturing action of urea and guanidine hydrochloride towards two thermophilic esterases. Biochem J 2002;367:857–863. [PubMed: 12160466]
61. Blancuzzi Y, Padilla A, Parello J, Cave A. Symmetrical rearrangement of the cation-binding sites of parvalbumin upon Ca2+/Mg2+ exchange. A study by 1H 2D NMR. Biochemistry 1993;32:1302–1309. [PubMed: 8095405]
62. Nara M, Tasumi M, Tanokura M, Hiraoki T, Yazawa M, Tsutsumi A. Infrared studies of interaction between metal ions and Ca(2+)-binding proteins. Marker bands for identifying the types of coordination of the side-chain COO- groups to metal ions in pike parvalbumin (pI = 4.10). FEBS Lett 1994;349:84–88. [PubMed: 8045307]
63. Kharakoz DP. Partial volumes and compressibilities of extended polypeptide chains in aqueous solution: additivity scheme and implication of protein unfolding at normal and high pressure. Biochemistry 1997;36:10276–10285. [PubMed: 9254626]
64. Jackson SE, Moracci M, elMasry N, Johnson CM, Fersht AR. Effect of cavity-creating mutations in the hydrophobic core of chymotrypsin inhibitor 2. Biochemistry 1993;32:11259–11269. [PubMed: 8218191]

65. Dragan AI, Read CM, Makeyeva EN, Milgotina EI, Churchill ME, Crane-Robinson C, Privalov PL. DNA binding and bending by HMG boxes: energetic determinants of specificity. J Mol Biol 2004;343:371–393. [PubMed: 15451667]

66. Henzl MT, Davis ME, Tan A. Divalent ion binding properties of the timothy grass allergen, Phl p 7. Biochemistry 2008;47:7846–7856. [PubMed: 18576674]

67. Garbuzynskiy SO, Kondratova MS. Structural features of protein folding nuclei. FEBS Lett 2008;582:768–772. [PubMed: 18258199]

68. Efimov AV. Favoured structural motifs in globular proteins. Structure 1994;2:999–1002. [PubMed: 7881910]

69. Streicher WW, Makhatadze GI. Unfolding thermodynamics of Trp-cage, a 20 residue miniprotein, studied by differential scanning calorimetry and circular dichroism spectroscopy. Biochemistry 2007;46:2876–2880. [PubMed: 17295518]

70. Schwaller B. The continuing disappearance of "pure" Ca2+ buffers. Cell Mol Life Sci 2009;66:275–300. [PubMed: 19099190]

71. Bernhisel-Broadbent J, Strause D, Sampson HA. Fish hypersensitivity. II: Clinical relevance of altered fish allergenicity caused by various preparation methods. J Allergy Clin Immunol 1992;90:622–629. [PubMed: 1401644]

72. Poirot O, O'Toole E, Notredame C. Tcoffee@igs: A web server for computing, evaluating and combining multiple sequence alignments. Nucleic Acids Res 2003;31:3503–3506. [PubMed: 12824354]

73. Declercq JP, Tinant B, Parello J, Etienne G, Huber R. Crystal structure determination and refinement of pike 4.10 parvalbumin (minor component from Esox lucius). J Mol Biol 1988;202:349–353. [PubMed: 3172221]

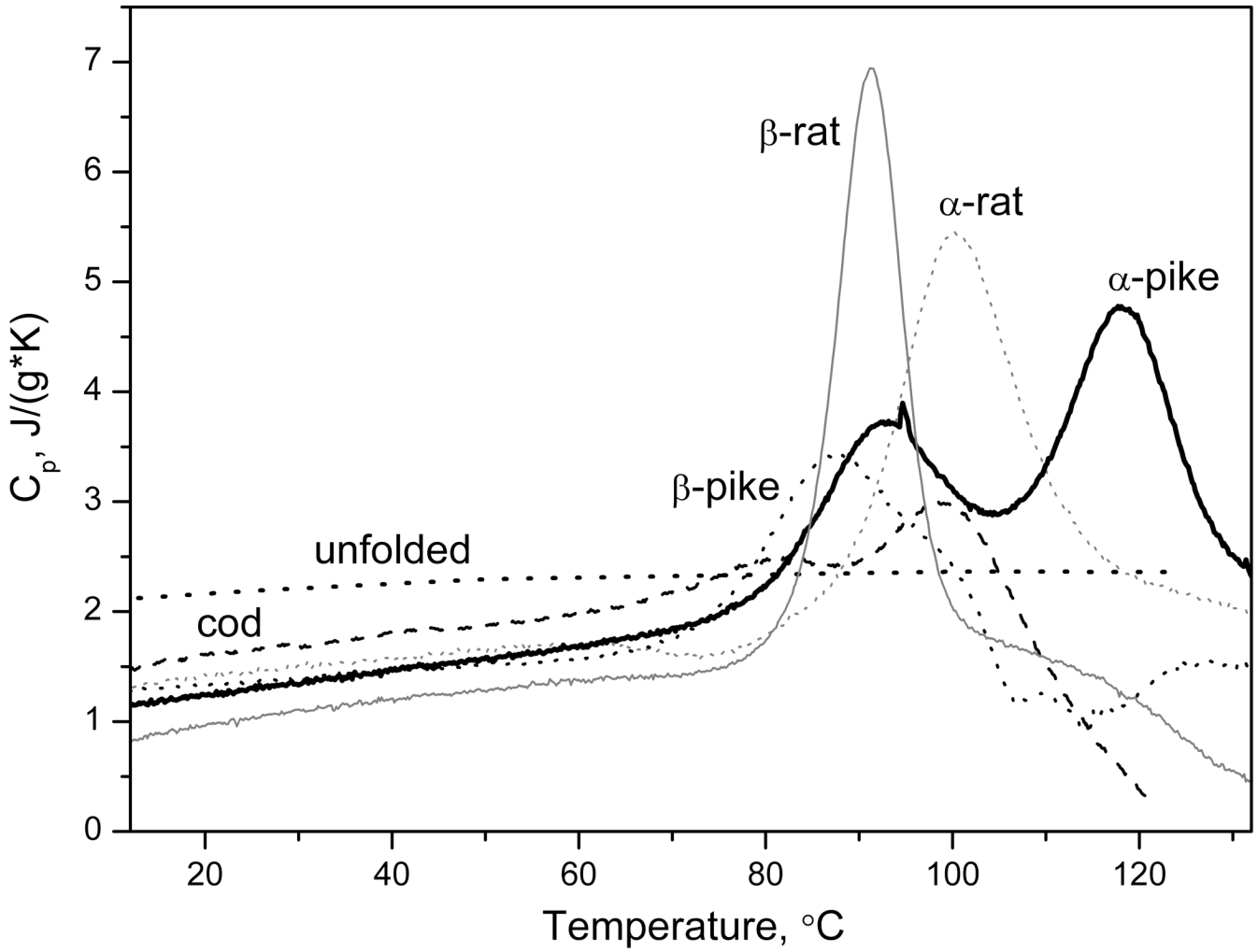

Figure 1.

Temperature dependence of specific heat capacity of Ca^{2+}-loaded (1 mM $CaCl_2$) parvalbumins from different organisms, estimated from DSC data (pH 8.1–9.0, 10 mM H_3BO_3-KOH). Heating rate was 1°C/min, protein concentration was 1.4–2.1 mg/ml. *Dotted curve* corresponds to the heat capacity of fully unfolded parvalbumins (deviation is within 0.05 J/(g*K)), as estimated according to Makhatadze *et al.* [36].

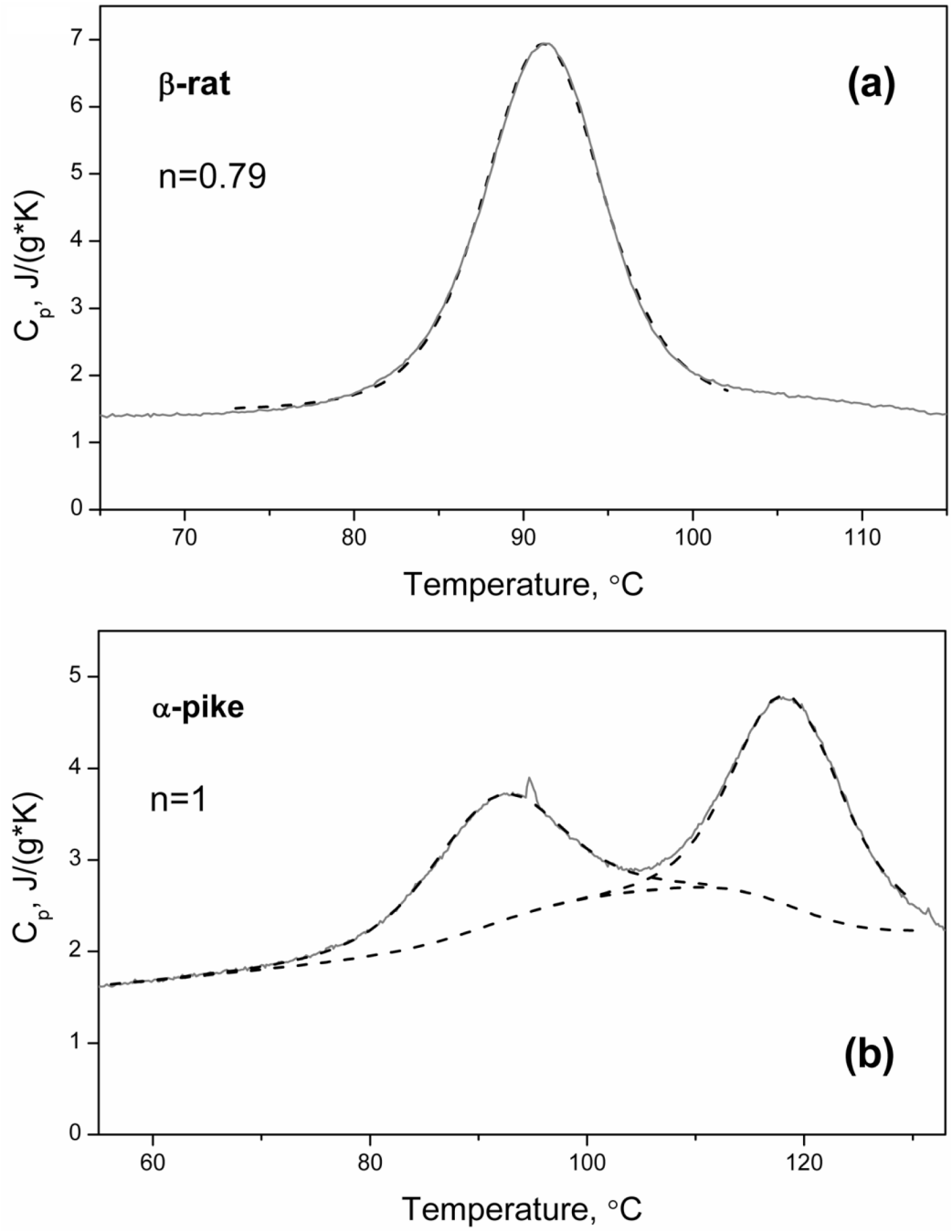

Figure 2.

Approximation of experimental DSC data (shown in Figure 1) for Ca^{2+}-loaded (1 mM $CaCl_2$) forms of rat β-parvalbumin **(a)** and α-isoform of pike PA **(b)** by theoretical curves computed according to the *cooperative two-state model* [1] and to the *model of two successive cooperative transitions* [2], respectively. The analysis of the data for pike PA was performed at fixed n value (n=1). The experimental and theoretical curves (Equations (1)–(4)) are shown solid and dashed, respectively.

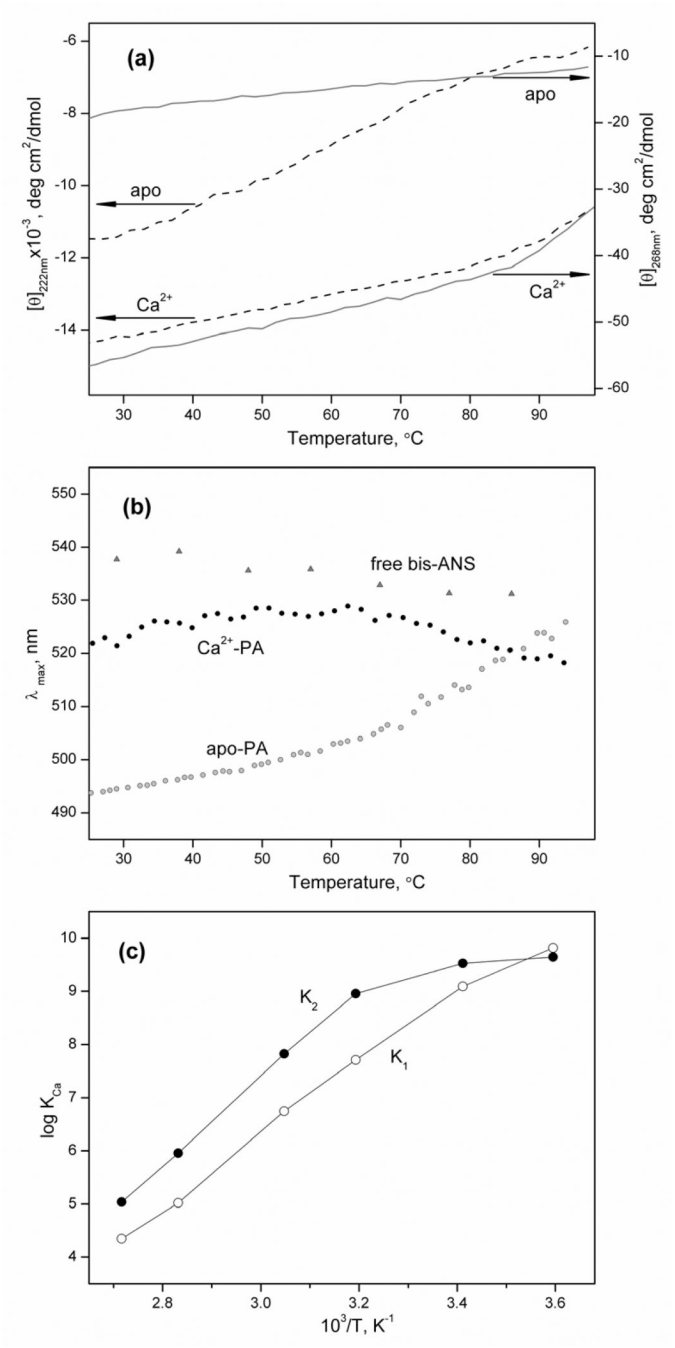

Figure 3.

Thermally induced changes of far- and near-UV ellipticity **(a)**, fluorescence spectrum maximum position (λ_{max}) of hydrophobic probe bis-ANS **(b)** for apo- (1.5–3 mM EDTA) and Ca^{2+}-loaded (1 mM $CaCl_2$) forms of pike α-PA, and temperature dependence of equilibrium Ca^{2+} association constants for pike α-PA, estimated from the fit of spectrofluorimetric Ca^{2+}/EDTA titrations of apo-protein according to the sequential Ca^{2+} binding scheme [3] **(c)**. Buffer conditions: pH 8.7, 10 mM H_3BO_3, or pH 8.0–8.2, 10–20 mM HEPES. K^+ was used as a counter ion in the buffer systems. Protein concentrations: 5–10 μM and 130–220 μM for far- and near-UV CD experiments, respectively; 20 μM and 8–14 μM for bis-ANS and PA fluorescence measurements, respectively. In the near-UV CD and titration experiments Ca^{2+}

was depleted using the gel-filtration method described by Blum *et al.* [33]. Bis-ANS concentration was 2 μM. The excitation wavelength was 385 nm or 259 nm for bis-ANS and PA fluorescence measurements, respectively.

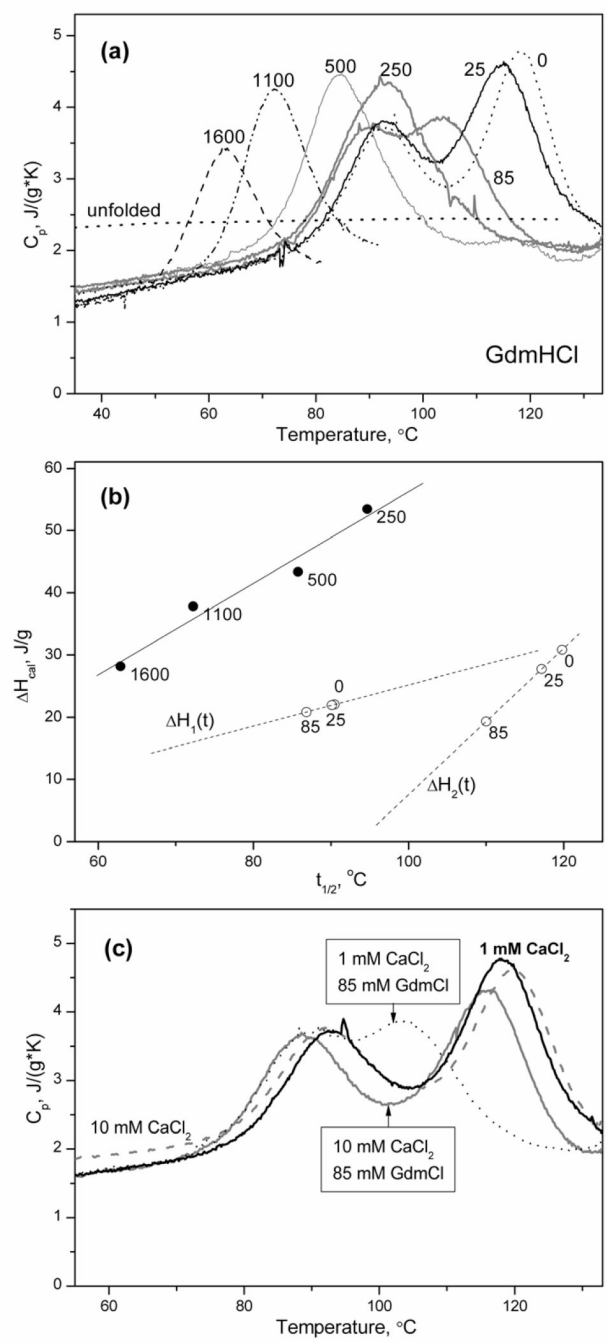

Figure 4.

The effects of GdmCl on the DSC heat sorption curves of Ca^{2+}-loaded (1 mM $CaCl_2$) pike α-PA **(a)**, thermodynamic analysis of the calorimetry data **(b)**, and $CaCl_2$-induced reversal of GdmCl action **(c)**. Buffer conditions: pH 9.0, 10 mM H_3BO_3-KOH. Heating rate was 1°C/min; protein concentration was 1.5–.1 mg/ml. The numbers indicate the concentrations of GdmCl in mM. (a) Dotted curve corresponds to the heat capacity of fully unfolded protein, as estimated according to Makhatadze *et al.* [36]. (b) The calorimetric curves exhibiting a single heat sorption peak (250–1600 mM GdmCl) or two distinct peaks (0–85 mM GdmCl) were approximated by theoretical curves computed according to the *cooperative two-state model* [1] or to the *model of two successive cooperative transitions* [2] (*fixed n=1*), respectively. The

thermal denaturation enthalpy (ΔH_{cal}) and mid-transition temperature ($t_{1/2}$) were estimated from the fit of the experimental data on figure (a) according to the Equations (1)–(4). The experimental dependencies of ΔH_{cal} upon $t_{1/2}$ were approximated by linear functions. $\Delta H_1(t)$ and $\Delta H_2(t)$ denote the lines, corresponding to the first and second thermal transitions in pike α-PA, respectively.

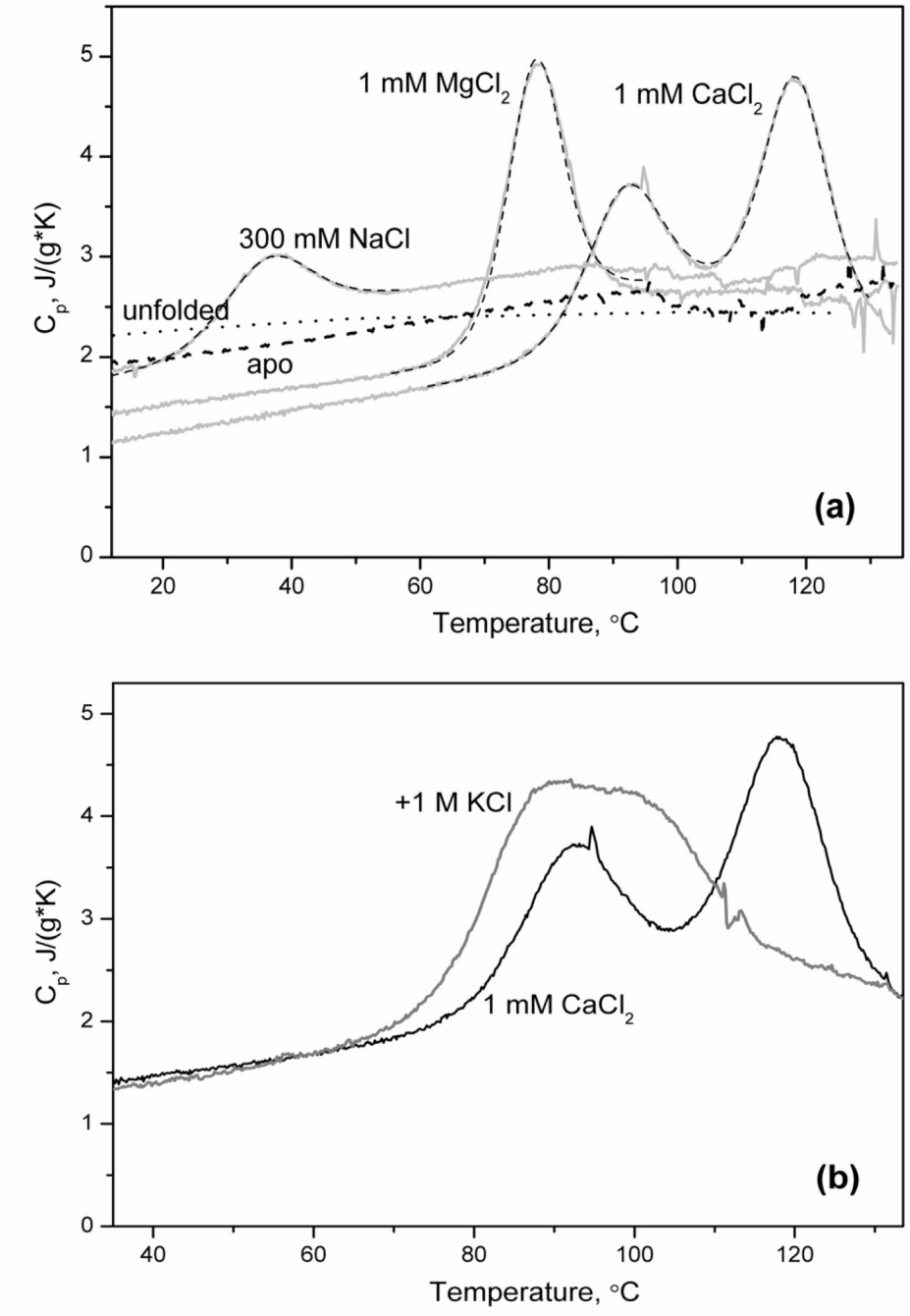

Figure 5.

The dependence of the DSC thermogram for pike parvalbumin α-isoform on the type of metal cation bound (pH 9.1, 10 mM H_3BO_3-KOH or 20 mM glycine-KOH). Heating rate was 1°C/min, protein concentration was 1.7–2.2 mg/ml. Calcium ions were depleted from PA using the Sephadex G-25 gelfiltration method described by Blum *et al.* [33]. The analysis of DSC data for metal-bound PA (*solid curves*) was performed according to the *cooperative two-state model* [1] (for Na^+- and Mg^{2+}-bound forms) or to the *model of two successive cooperative transitions* [2] (for Ca^{2+}-form) using n=1 (Equations (1)–(4); *dashed curves*). *Dotted curve* corresponds to the heat capacity of fully unfolded protein, as estimated according to Makhatadze *et al.* [36].

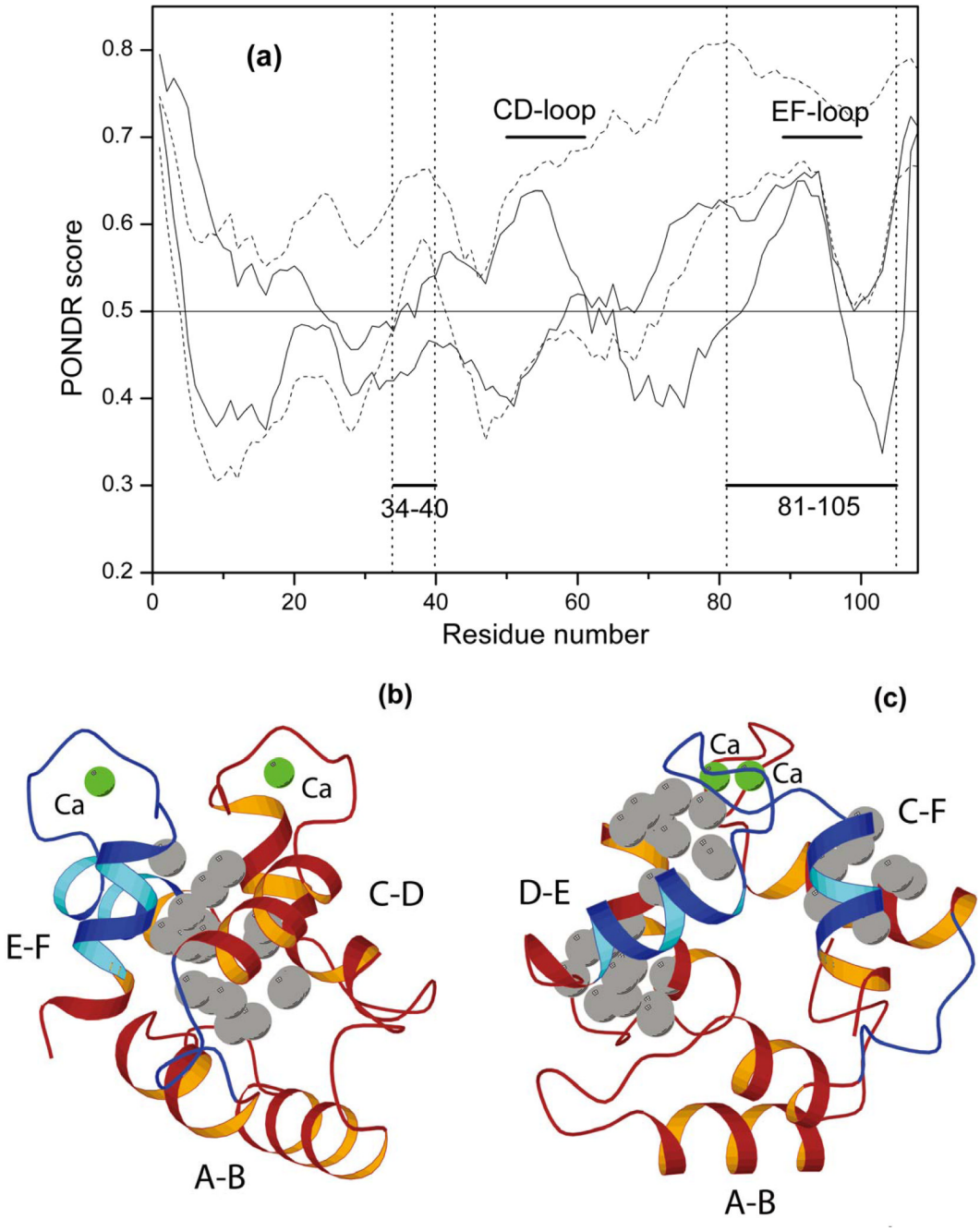

Figure 6.

The ranges of possible PONDR score values for parvalbumins, possessing either one (PAs of group 1; *dashed curves*) or two (group 2; *solid curves*) heat sorption peaks in the Ca^{2+}-bound form **(a)**; spatial distribution of atoms forming two types of cavities (shown space-filled in grey) in pike α_2-PA: central cavities (formed by atoms provided by at least three out of four helices C, D, E, F) **(b)**; cavities formed by atoms provided by either D and E helices (including DE loop) or C and F helices **(c)**. (a) The group 1 includes two rat PAs and carp protein; group 2 consists of pike α_1-PA and cod protein. The PA sequences were treated using PONDR®-VSL1 algorithm [41,42], followed by alignment with T-COFFEE online service [72]. The numbering of residues is based upon the amino acid sequence of pike α_2-PA. The residue

numbers for fragments of PAs from group 2 having confidently lowered compared to PAs of group 1 PONDR values (higher probability of being in folded conformation) are marked in figure (a) and the respective residues are shown on figures (b) and (c) in blue. (b) and (c) Cavities were calculated from X-ray structure of Ca^{2+}-bound form of pike α_2-PA (PDB code 1PVA [47,73], chain A) using CASTp server [51]. Calcium ions are in green. Figures were prepared with MolScript [52].

Table 1

Thermodynamic parameters describing thermal denaturation of various parvalbumins, estimated from DSC data (Figure 1, Figure 2, Figure 4, Figure 5) according to either the *cooperative two-state model* [1] (Equations (1) and (2)) or the *model of two successive cooperative transitions* [2] (Equations (3) and (4)). The indexes 1 and 2 refer to the parameters describing the first (low-temperature) and second heat-sorption peaks, respectively.

Protein	Solvent conditions	ΔH_0, J/g		T_0, K		ΔC_p, J/(g•K)		n
		$\Delta H_{0,1}$	$\Delta H_{0,2}$	$T_{0,1}$	$T_{0,2}$	$\Delta C_{p,1}$	$\Delta C_{p,2}$	
Pike α	1 mM $CaCl_2$	22.4	31.0	363.6	393.0	0.49	−0.78	1
Pike α	10 mM $CaCl_2$	22.3	29.9	363.7	394.9	0.31	−0.91	1
Pike α	1 mM $CaCl_2$, 1 M KCl	33.8	32.1	360.6	377.0	0.16	−0.31	0.59*
Pike α	1 mM $CaCl_2$, 85 mM GdmCl	20.9	19.4	360.0	383.2	0.66	−1.22	1
Pike α	10 mM $CaCl_2$, 85 mM GdmCl	23.1	28.7	360.5	391.6	0.30	−1.10	1
Pike α	1 mM $MgCl_2$	30.1		350.4		0.57		1
Pike α	300 mM NaCl	12.8		306.2		0.47		1
Pike β	1 mM $CaCl_2$	21.9		358.0		0.58		1
Rat α	1 mM $CaCl_2$	49.0		373.3		0.26		0.53*
Rat β	1 mM $CaCl_2$	49.8		364.5		−0.24		0.79*

*n value is used as an additional fitting parameter

Table 2

The characteristics (S, area; V, volume) of cavities of pike α_2, rat α and β and carp pI 4.25 parvalbumins (PDB codes 1PVA, 1RWY, 1RRO and 4CPV, respectively), estimated using CASTp server [51]. The successive triplets of columns correspond to the following sets of cavities: 1) all cavities found; 2) central cavities (formed by atoms provided by at least three out of four helices C, D, E, F); 3) cavities formed by atoms provided by either D and E helices (including DE loop) or C and F helices; 4) cavities formed by atoms provided by B and D helices.

Protein	Total number of cavities	S ($Å^2$)	V ($Å^3$)	Number of central cavities	S ($Å^2$)	V ($Å^3$)	Number of D–E and C–F cavities	S ($Å^2$)	V ($Å^3$)	Number of A–B–D or B–D cavities	S ($Å^2$)	V ($Å^3$)
Pike α	9	398	215	3	195	108	4	143	76	1	34	18
Rat α	6	265	153	1	76	56	2	72	39	1	50	25
Rat β	4	158	92	1	51	33	2	78	46	1	28	14
Carp pI4.25	6	222	126	1	72	50	4	119	60	1	31	16